remote sensing

MDPI

Article

Effects of Viewing Geometry on Multispectral Lidar-Based Needle-Leaved Tree Species Identification

Brindusa Cristina Budei [1,2,*], Benoît St-Onge [3], Richard A. Fournier [4] and Daniel Kneeshaw [5]

[1] Environmental Sciences Institute, Université du Québec à Montréal (UQAM), Montreal, QC H3C 3P8, Canada
[2] Centre d'Enseignement et de Recherche en Foresterie de Sainte-Foy (CERFO), Quebec, QC G1V 1T2, Canada
[3] Geophoton Inc., Montreal, QC H3X 2T3, Canada
[4] Department of Applied Geomatics, CARTEL, Université de Sherbrooke, Sherbrooke, QC J1K 2R1, Canada
[5] Department of Biology, Université du Québec à Montréal (UQAM), Montreal, QC H3C 3P8, Canada
* Correspondence: budei.brindusa_cristina@courrier.uqam.ca

Abstract: Identifying tree species with remote sensing techniques, such as lidar, can improve forest management decision-making, but differences in scan angle may influence classification accuracy. The multispectral Titan lidar (Teledyne Optech Inc., Vaughan, ON, Canada) has three integrated lasers with different wavelengths (1550, 1064 and 532 nm), and with different scan angle planes (respectively tilted at 3.5°, 0° and 7° relative to a vertical plane). The use of multispectral lidar improved tree species separation, compared to mono-spectral lidar, by providing classification features that were computed from intensities in each channel, or from pairs of channels as ratios and normalized indices (NDVIs). The objective of the present study was to evaluate whether scan angle (up to 20°) influences 3D and intensity feature values and if this influence affected species classification accuracy. In Ontario (Canada), six needle-leaf species were sampled to train classifiers with different feature selection. We found the correlation between feature values and scan angle to be poor (mainly below $|\pm 0.2|$), which led to changes in tree species classification accuracy of 1% (all features) and 8% (3D features only). Intensity normalization for range improved accuracies by 8% for classifications using only single-channel intensities, and 2–4% when features that were unaffected by normalization were added, such as 3D features or NDVIs.

Keywords: tree species identification; multispectral lidar; scan angle; lidar intensity; Titan; random forest; forestry

Citation: Budei, B.C.; St-Onge, B.; Fournier, R.A.; Kneeshaw, D. Effects of Viewing Geometry on Multispectral Lidar-Based Needle-Leaved Tree Species Identification. *Remote Sens.* **2022**, *14*, 6217. https://doi.org/10.3390/rs14246217

Academic Editors: Sheng Nie, Chenglu Wen, Di Wang, Xuebo Yang and Shaobo Xia

Received: 12 October 2022
Accepted: 5 December 2022
Published: 8 December 2022

1. Introduction

Individual tree species identification is important for precise forest management, and several studies have evaluated identification methods that are based upon discrete small footprint airborne lidar alone [1–8] or in combination with passive multispectral imagery [9–13]. Airborne multispectral lidar recently has been proposed as an improvement over single-sensor technology for identifying tree species [14–16].

Single-tree species identification using lidar data has generally been performed in three steps. First, single-tree crowns are delineated, after which the corresponding lidar point clouds are extracted. Second, for each single-tree point cloud, features are calculated from return heights (3D features), and from return intensities (intensity features). Third, a classifier (e.g., random forest, RF) is trained using reference tree crowns of known species to compute a classification model, which is then applied to target tree crowns to identify the species. One of the underlying assumptions of this approach is that the location of trees relative to the laser scanner has no effect on their point cloud features. However, scan angle, which determines the incidence angle of the laser pulses on the trees, may affect the values of the computed features, consequently influencing the accuracy of species identification. The majority of airborne lidar systems allow large maximum lateral scanning angles (up to ±30°) to help reduce acquisition costs. Yet, in forestry applications lidar service providers

frequently propose maxima of ±15° to 20° to avoid bias at larger scan angles. In addition to lateral scan angles, a multispectral lidar, such as the Titan system of Teledyne Optech Inc. (Vaughan, ON, Canada), may have lasers scanning the same tree using different scanning planes (e.g., with forward tilted scanning planes). The combination of across-track and along-track angles increases the resulting scan angles (hereafter referred to as "net" scan angle). Multispectral airborne lidar is usually considered advantageous because it collects intensities at different wavelengths, which should improve tree species separation compared to single-laser systems. Furthermore, it not only provides different single-channel intensity classification features, but also increases the possibility of computing ratios and normalized differences, as well as 3D features that are enhanced by the greater point density [14–19]. While providing richer spectral information, one inconvenient aspect of the system is that it produces data with variable acquisition geometries between channels (i.e., larger net scan angles and no vertical view for two of the three channels in the case of the Titan system). This potentially increases scan angle influence on 3D and intensity features compared to mono-spectral lidar (i.e., a scanner using only a vertical scanning plane).

Individual tree crown (ITC)-level 3D and intensity features are highly variable because they are influenced by multiple elements, some of which depend upon tree characteristics (species, height, stress, tree shape, vertical and horizontal distribution of vegetation within the crown, clumping and occlusion, leaf density, leaf angles, phenological state), together with each tree's environment (tree status, surrounding tree density, topography, understory). Features also depend upon laser properties (pulse power, pulse divergence, wavelength, range, scan angle), and on the configuration of the survey (pulse density, flight altitude, lateral overlap, flight lines configuration, maximum scan angle). Several of these elements influence ITC features in a manner that is not independent of scan angle, possibly producing cumulative effects and increasing feature variability. A priori, it is difficult to isolate the respective influences of all elements.

The difficulty of isolating and understanding the specific scan angle influence from among other influencing factors has been highlighted in studies adopting an Area-Based Approach (ABA). These studies have used either simulated lidar in of modelled trees or real lidar data [20–27]. As the influence of scan angles up to 20° on ABA features (e.g., canopy height) has not been found to be very large, scan angle has been ignored in most studies [20–22,28,29]; nevertheless, its potential influence on forest-feature accuracy is frequently mentioned [27].

The sensitivity and variability of ITC features are greater than those of ABA features, given that the ITC volume in which laser pulses can be intercepted is smaller than that of ABA cell volume. Thus, we highlight the specific need to study ITC feature value variations with scan angle, even for relatively small scan angles, i.e., up to +/−20°. The studies that are specifically addressing the effect of scan angle on tree features at ITC level are mainly based upon simulation models using geometric representations of trees [30]. Very few studies have employed real lidar data [31]. So far, we could not find any study that specifically assessed the influence of scan angle on multispectral features at the ITC level using real airborne lidar data.

Large scan angles (large deviations from the vertical) produce at least three effects. First, large angles cause a decrease in return intensity that is due to both the increase in laser range and footprint size. Consequently, the pulse energy per unit area reaching the top of the canopy decreases [32,33]. The effect of this attenuation (effect #1) is more pronounced for beams having a large divergence. Second (effect #2), large scan angles cause a decrease in the number of returns per emitted pulse (i.e., receiving multiple returns from a given pulse becomes less likely), which in turn produces a higher proportion of single returns. Third (effect #3), large scan angles cause a change in the distribution of returns through the forest canopy along the pulse trajectory. A decrease in the peak pulse power concentration at the top of the canopy alters the shape and amplitude of the signal, given that more

vegetation material is needed to trigger a return. Thus, pulses penetrate deeper, and the height of returns is shifted downward [33].

The decrease in return intensity at larger scan angles changes the values of intensity percentiles (effect #1). In addition, the change in return proportions (effect #2) affects these features, especially when computed from all returns, because the number of second and third returns (having a reduced intensity) is larger at the nadir than at larger scan angles. Even if intensity normalization would compensate for the intensity decrease (effect #1), rigorous radiometric calibration, in practice, is very difficult for lidar intensity. Intensity normalization for vegetation returns through physical modelling is very complex because many factors have to be accounted for, such as range-related factors (laser spread loss and attenuation by air), or tree-related factors (leaf reflectance, leaf size and orientation). Different physical equations have been proposed to empirically normalize return intensities to compensate for range variations [34–36]. These equations theoretically allow the isolation of the scan angle effect as a function of range. More complex calibration methods introducing additional information for the purpose of retrieving radiometric characteristics [37–40] would make it more difficult to isolate the scan angle effect. The specific effect of intensity normalization as a function of range in reducing feature variability has been tested on the feature values themselves [41–43] or through the degree of improvement in tree species classification accuracy [34]. Moreover, even simple range normalization is technically difficult to apply to data that are distributed in the widely used LAS format because of the lack of information regarding pulse range.

No corrections have been proposed for effects #2 and #3 because these effects mainly concern second or third returns that are controlled by complex species-specific interactions between laser pulses and leaves or branches. Effect #2 mainly affects LiDAR features that are computed from return proportions, e.g., ratio of single to multiple returns, ratio of canopy to ground returns or the ratios of returns above a threshold of all returns; it has been highlighted in several studies using the ABA (i.e., at the plot-level) for canopy cover [23–25,29,44,45] or gap fractions [24–27,46].

Changes in return height distributions (effect #3) have been shown to influence lidar features, such as ABA height percentiles [20–22,24,28,29,32,46–49]. Some of these studies show that the two opposing effects of scan angle (shifting the height percentiles upward or downward) are not only related to forest density and occlusions, but they are also species-specific. For example, height percentiles varied more for species with deeper tree crowns relative to crown diameter, such as spruce (*Picea* spp.), compared to species with shorter crowns, such as pines (*Pinus* spp.), given the probability of intercepting oblique pulses [44]. Simulation studies also have explained the upward shift by the increased distance along which the beams must travel through the canopy, thereby producing an increase in the interception probability of pulses at large incidence angles [30,32,50]. The upward shift is further related to effect #2 by which a decrease in the number of returns per pulse influences the height percentiles that are calculated from all returns [49]. Overall, the three effects, which remain difficult to correct, influence feature values. In turn, feature values would affect species identification accuracy. The main objective of this study is to quantify the effect of scan angle on individual tree species identification, from feature calculation to classification, using real tree data and to evaluate the improvement brought about by range normalization of intensity. To do this, we addressed four specific objectives: (i) investigation of the effect of scan angle on 3D and intensity features that are used to identify species; (ii) identification of the species for which features are most sensitive to scan angle; (iii) evaluation as to whether scan angle affects the accuracy of species classification; and (iv) evaluation of the effect of intensity normalization per feature type and per mean scan angle on the accuracy of species identification.

2. Materials and Methods

2.1. Study Area and Reference Data on Tree Species

The study area is located in the York Regional Forest (YRF) of southern Ontario, Canada (79°19′W, 44°04′N), in the Great Lakes–St. Lawrence forest region [51]. The topography is mostly flat, with a terrain elevation range of about 43 m (240 m to 303 m). The forest stands in the study area are either naturally growing, mixed species stands or needle-leaf reforested/planted stands. We sampled six needle-leaf species that were found in plantations of different ages: red pine (*Pinus resinosa*); eastern white pine (*Pinus strobus*); Scots pine (*Pinus sylvestris*); tamarack or eastern larch (*Larix laricina*); Norway spruce (*Picea abies*); and white spruce (*Picea glauca*). The trees in this study were sampled mainly from needle-leaf plantations. Trees in plantations typically have similar characteristics, given that they are even-aged and grow under similar conditions. Because of this homogeneity, this dataset facilitates the isolation of the scan angle effect from other tree characteristics. For example, in more complex environments, such as natural stands or mixed stands that are composed of both needle-leaf and broadleaf species, trees grow in a wider variety of shapes and sizes, in dominant, sub-dominant or suppressed positions. These heterogeneous conditions could hinder separating scan angle effects from tree effects. Field identification of tree species was conducted in August 2015 to produce a reference database of individual trees within the study plantations. High-resolution (10 cm) images that were acquired during the Titan survey with the CM-1000 RGB camera (Teledyne Optech Inc., Vaughan, ON, Canada) were used to identify additional reference trees or to verify tree species in plantations using photo-interpretation.

The large sample tree dataset that was used in this study permits readily identifiable statistical trends, given that tree characteristics, occlusions and other flight parameters might exert greater effects on lidar features than would the scan angles if the number of sample trees was limited. Moreover, this study took advantage of multiple overlapping flight lines and the high return density of the Titan dataset, which allowed computing advanced features for multiple single flight line views of each tree.

2.2. Lidar Data and Intensity Correction for Range

The Titan system (Teledyne Optech Inc., Vaughan, ON, Canada) has three integrated lasers (hereafter referred as channels C1, C2 and C3) with different wavelengths (respectively, 1550, 1064 and 532 nm for C1–C3), and different scan angle planes, which are respectively tilted at 3.5°, 0° and 7° relative to the vertical plane. The data were acquired on July 2015 over an area of 2546 ha, at a mean altitude of about 800 m above the ground surface. The mean number of first returns per m^2, by channel and by individual flight line was 3.4 for C1 and C2, and 3.3 for C3, which is equivalent to a total of 10 returns per m^2 for all channels within a single flight line. At a range of 800 m, the average footprint at nadir was 28 cm for C1 and C2, and 56 cm for C3. Ranges and footprint diameters are summarized in Table 1. A total of 19 flight lines were acquired, with an average lateral overlap of 50%, thereby providing two views of each tree from different angles. Most flight lines were acquired following parallel centrelines, but in one area additional flight lines were acquired perpendicularly. These two orientations (north-south and east-west) locally increased the number of views per tree with different scan angles.

Table 1. Summary statistics of laser range and footprint diameter.

	Channel	Min	1st Quartile	Median	Mean	3rd Quartile	Max
Range (m)	C1	724	784	808	812	842	924
	C2	723	781	804	811	844	923
	C3	728	783	810	815	847	929
Footprint diameter (cm)	C1	25.34	27.45	28.27	28.43	29.48	32.34
	C2	25.30	27.34	28.14	28.39	29.54	32.29
	C3	50.96	54.82	56.69	57.01	59.26	65.03

Manual delineation of sampled crowns was performed on the canopy height model (CHM), which was generated using the highest returns of the three channels above the digital terrain model (DTM), within 10 cm pixels. Tree delineation followed the procedure that was proposed by Budei [14]. A colour composite image that was generated by interpolating the first return intensity of each of the three channels was used to verify species and delineation, especially when two trees of different species were difficult to separate from the 3D information alone. The DTM was calculated from all ground returns that were amassed from all channels and all flight lines. This allowed us to produce a single DTM (ground reference) for all three channels and for all flight lines. A similar approach was used for tree height calculations: individual tree heights were calculated using all first returns.

Lidar data that were acquired with the Titan system were obtained both in LAS 1.3 and ASCII formats. The latter contained additional information on laser range and provided more precise scan angle data than did the integer values in degrees that were provided in the LAS files. The laser range information allowed us to normalize intensity following the equation that was proposed by Korpela [34]:

$$I_n = \left(R/R_{ref}\right)^a I_{raw} \quad (1)$$

where I_n is the range-normalized intensity, I_{raw} is the raw intensity, R is the range, and R_{ref} is the reference range. The exponent a was set to 2.0.

2.3. Net Pulse Scan Angles

The maximum lateral scan angle (mirror angle) for each of the three channels was about $\pm 15^{\circ}$. The tilt of the non-vertical sensor scanning planes of two of the Titan lasers increased the net scan angle. This net scan angle was calculated from the angle along the scanning plane (mirror angle), and the angle of the sensor-scanning plane (tilt) (Figure 1). The high precision data on the mirror scan angles (in degrees, to 5 decimal places) that were provided in the ASCII files were used for this purpose. Yet, information on the sensor orientation for each pulse (roll and pitch) or flight trajectories was not available. Therefore, roll and pitch of the aircraft were considered to be equal to zero. We consider these assumptions to be reasonable since the wind speed during the flight was under 11 km/h, and because there are no visual variations in the horizontal return distributions along the flight path. We used the following equation to calculate the net angle (γ) from the mirror scan angle (α) and the scanning plane tilt (β):

$$\gamma = atan\sqrt{tan^2(\alpha) + tan^2(\beta)} \quad (2)$$

Hereafter we use "scan angle" to designate the net angle as calculated with Equation (2). It was calculated for Titan channels 1 and 3, given that channel 2 had zero tilt. The "incidence angle", which is largely used in studies concerning backscattered signals from a scanned object [32,33,45,52], assumes an accurate measure of the scan angle and of the normal to the local surface (often calculated from the DTM). Yet, the use of the term "incidence angle" was considered inappropriate in this study, given that the exact aircraft attitude parameters (roll, pitch and yaw) were not known; consequently, the true incidence angle relative to the horizontal plane at tree level could not be precisely calculated. Furthermore, the normal of a tree crown at the position of a lidar return is difficult to define.

Across overlapping flight lines, each tree was scanned from multiple angles. For the sake of simplicity, a scan of a single tree from a single flight line (point of view) is named a "tree view". A given tree view comprises the three point clouds respectively corresponding to each of the three Titan channels. For each tree view, different mean scan angles were calculated (see details in Section 2.4). Figure 2 highlights the difference in point cloud configuration according to mean scan angle in C2 for an individual *Pinus resinosa*.

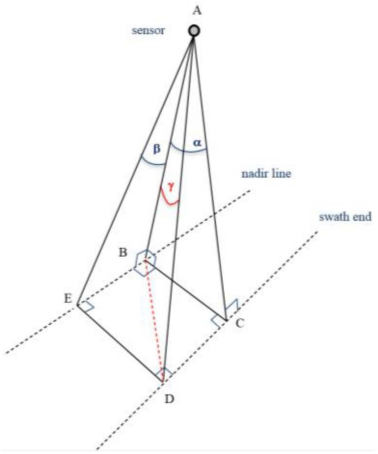

Figure 1. Calculation of net scan angle γ ($B\hat{A}D$). A represents the sensor position. B represents the nadir point or the point return at zero mirror scan angle in vertical channel C2. E represents the point return at zero mirror scan angle in tilted channels C1 or C3. α = mirror scan angle ($B\hat{A}C = E\hat{A}D$). β represents the inclination of the scanning plane (here EAD plane) for any of the tilted channels (C1 or C3). BC = ED represents the distance between the nadir line (BE) and the interception position (C or D) when mirror scan angle = α.

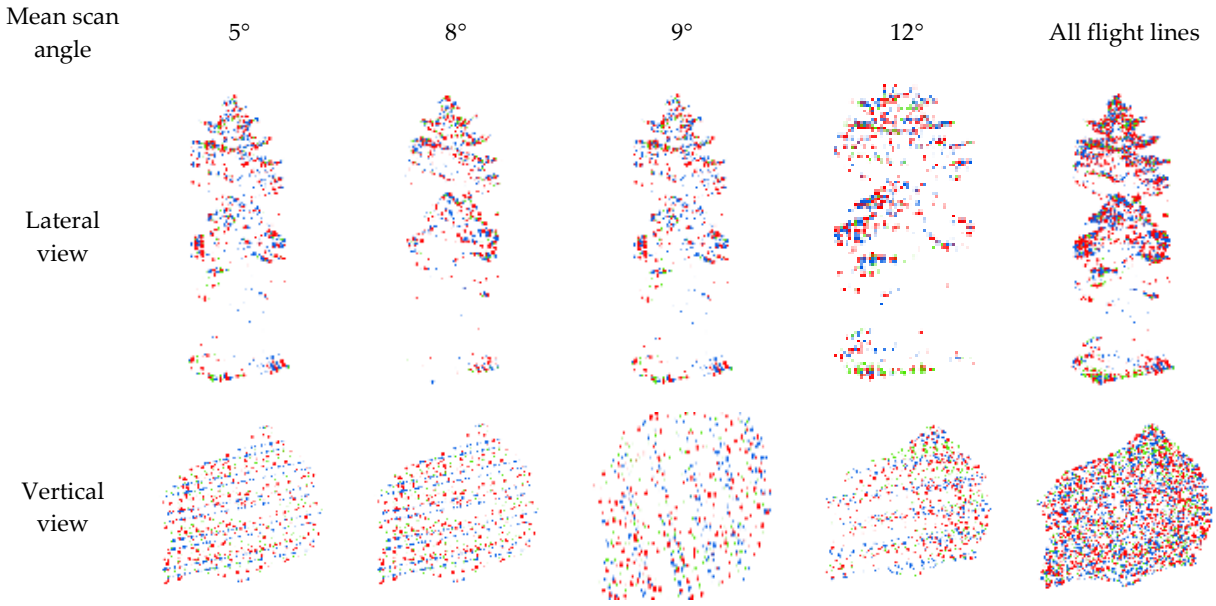

Figure 2. Example of the point cloud of a *Pinus resinosa* tree as seen from four different flight lines with respective scan angles of 5°, 8°, 9° and 12° (i.e., four tree views), and a combination of the point clouds from all four flight lines. Mean scan angle of the individual tree views was calculated from C2. Legend: red = C1, blue = C2, green = C3; point size is a function of intensity.

The 3D and intensity features were computed for each reference tree. Several versions of each feature were computed from the point cloud that was extracted for each channel of each tree view. A feature version corresponds to one of three return types: all returns (all); first returns (1st); and single returns (si). A variable threshold for each tree was used to remove potential ground and understory points by retaining only returns that were greater than 40% of the height of the reference trees.

The 3D features were calculated using the normalized height above the ground of crown returns. A unique value of ground, the DTM pixel value at the tree crown centroid, was used to calculate return heights for all returns of the tree to avoid altering the crown return height distribution on sloping terrain. Height normalization consisted of dividing

the height of each return by that of the highest return of the corresponding crown. The same raster DTM was used for the calculation of all features. The 3D features were calculated for each single channel (C1, C2, C3), as well as for the three channels combined (C321). The features included the mean (mn), the relative height at certain percentiles (PE, 5th, 10th, 25th, 50th, 75th, 90th and 95th percentiles: p05, p10, p25, p50, p75, p90, p95), the return height distribution (DI, i.e., standard deviation: sd; coefficient of variation: cv; skewness: skew, and kurtosis: kurt), the ratios of features that were calculated from different return types (RM, e.g., 1st returns mean height divided by tree height), and crown taper (SL, mean of the slope between each return and the highest return within a tree). We also computed the ratios of the number of returns of different types (Return Proportion—RP, e.g., the ratio of the number of first returns over that of all returns, etc.), which we have included with 3D features.

For comparison purposes, the intensity features were computed from raw intensities, as well as from the range-normalized intensities. Most intensity features were computed from individual channels (e.g., mean intensity, intensity percentiles). Other intensity features consisted of simple ratios of intensities between two channels (Ratio Channels or RC, two ratios using the green (G) channel: RCG1 from C2/C3 channels combination, RCG2 from C1/C3, and the third ratio using only infrared (IR) channels: RCIR from C1/C2), or normalized differences (ND, NDG1 as (C2 + C3)/(C2 − C3), NDG2 and NDIR from corresponding channels). For a complete description of features and their acronyms, see Budei [14] and Budei and St-Onge [18]. A description of the features is also provided in Table 2.

Table 2. Feature description.

Type	Symbol	Description
Structure	AH	Ratio of crown Area to tree Height
3D	DI	DIspersion: coefficient of variation (cv), skewness (skew), kurtosis (kurt) of return heights
	HR	The slope coefficient of a linear model fit to the values of mean Height of returns that XY position fit in each of four concentric and equidistant Rings, which are centred on the highest return location (lm), and coefficient of variation of the mean height by ring (cv)
	MH	Mean of normalized Height
	PE	PErcentiles of normalized height
	RB	Ratio of the number of returns in different height Bins defined in % of tree height to the total number of returns (e.g., 60_80 is the ratio of the number of returns in the 60-80% bin to all the returns in a crown)
	RM	Ratio between different statistics or Metrics: - 1st returns mean height/tree height (1st_mn) - 1st returns median height/tree height (1st_p50) - 1st returns median height/1st returns mean height (1st_p50_1st_mn) - all returns mean height/tree height (all_mn) - all returns median height/tree height (all_p50) - all returns median height/1st returns mean height (all_p50_mn) - 1st returns median height/all returns mean height (1st_p50_all_mn) - 1st returns mean height/all returns mean height (1st_mn_all_mn) - 1st returns mean height/2nd returns mean height (1st_mn_2nd_mn)
	RP	Return Proportion: - ratio of first returns to all returns - ratio of single returns to first returns
	SL	The average SLope of the lines connecting the highest return to each other returns
	SU	Sum of the two quadratic coefficients (coef) of a least-squares SUrface fit, and average of absolute vertical residual values of the above fit divided by the height of tree (rs)

Table 2. *Cont.*

Type	Symbol	Description
Intensity	DI	DIspersion: Standard deviation, coefficient of variation, skewness, kurtosis
I	IR	Intensity by concentric Ring centered on the highest return
	MI	Mean of Intensity
	NDG1	Green (type 1) Normalized Difference Vegetation Index: [C2 − C3]/[C2 + C3]
	NDG2	Green (type 2) Normalized Difference Vegetation Index: [C1 − C3]/[C1 + C3]
	NDIR	InfraRed Normalized Difference Vegetation Index: [C1 − C2]/[C1 + C2]
	PE	PErcentiles
	RCG1	Green Ratio of Channels (type 1): C3/C2
	RCG2	Green Ratio of Channels (type 2): C3/C1
	RCIR	InfraRed Ratio of Channels: C2/C1
	RM	Ratio between different statistics or Metrics. - 1st returns mean intensity/all returns mean intensity - (1st_ p50_all_ p50) - 1st returns mean intensity/2nd returns mean intensity - (1st_p50_2nd_p50)

Abbreviations: mn = mean, cv = coefficient of variation, p = percentile, lm = linear model fit, 1st = first returns, all = all returns, 2nd = second returns).

2.4. Tree View Selection

Depending upon tree characteristics (tree height), tree environment (neighbour occlusion) or flight configuration (return density or position of the tree near the swath end), the number of returns by channel within individual flight lines was occasionally insufficient for calculating some of the features, leading to "non-applicable" (NA) values. The presence of NA could create bias in comparisons between the correlation coefficients of features that were calculated with different scan angles or between classification accuracies for different groups of tree views having a similar scan angle. Several a priori criteria were used to discard trees that would yield NA values in the features. For example, trees that were severely defoliated were not considered. Furthermore, only trees taller than 10 m were selected; below this threshold, the frequency of NA was too high. Furthermore, only trees that were sufficiently well scanned from at least two flight lines in three channels were selected. Tree views that were located at the extremity of the scan swath (that had a mean scan angle larger than $\pm 14^\circ$ in C2) were discarded. The main reason for this choice was that returns near the end of scan lines of an oscillating mirror that operated with a maximum scan angle of 15° have less precise geolocations and are not evenly distributed. They are closer together at the end of scan line when the oscillating mirror slows before reaccelerating in the opposite direction. In addition, the space between scan lines is greater at wider scan angles, leaving bigger gaps. Common practice is, therefore, to eliminate returns at the extremities of scan lines. Yet, in order to avoid computing features from point clouds that would be cut in the middle of tree views (i.e., in the middle of a tree crown) at the 14° scan angle threshold, we retained all tree views that had a mean scan angle of 14° or less in C2, but we kept the returns therein having a scan angle above 14°, if any. From a total of 37,063 candidate trees that had been manually delineated [18], 13,325 trees met all of the above selection criteria. This resulted in 27,922 tree views that were used for computing the correlation between feature values and mean scan angle, and for RF (random forest) classification. The tree views were divided into three scan angle classes (see Figure 3). Because of the position of these trees relative to the flight line, the frequency distributions of the mean scan angle of the tree views per channel differed between species (Figure 4). Therefore, we enforced a minimum of 30 tree views in each mean scan angle

class, and we applied a balanced RF algorithm (down sampling) to compensate for the difference in sample sizes between different species.

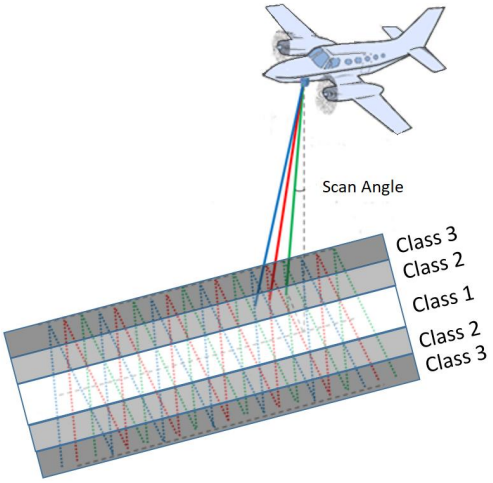

Figure 3. Configuration of scan angle classes from nadir (Class 1) to swath end (Class 3).

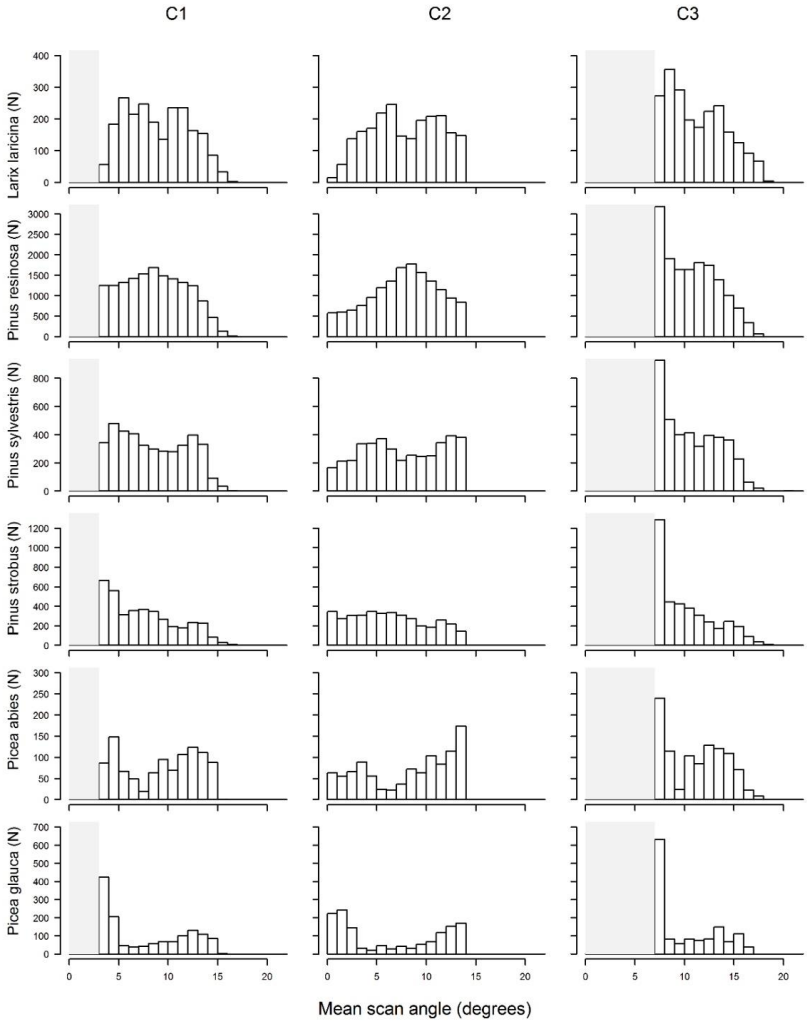

Figure 4. Distributions of mean scan angle of the tree views by channel (C1, C2 and C3) and species. The grey-shaded areas represent mean scan angles that are not achievable in the respective channels due to the Titan system's configuration.

2.5. Correlation between Feature Values and Mean Scan Angle

Each feature was computed for a specific combination of point clouds corresponding to different view geometries. For this reason, different mean scan angles were considered for each tree view, depending upon the specific combination of point clouds extracted from different channels (C1, C2, C3), or combinations of two or three channels (C1_C2, C2_C3, C1_C3 and C321). Combinations of two or three channels were calculated to understand the effect of scan angle on multi-channel feature values, such as channel ratios or NDVIs and 3D features. For single-channel features, the mean scan angle value of a tree view was computed using only the absolute scan angle value of all returns in that channel. For features that were constructed as channel ratios or NDVIs, the mean scan angle was first computed for each channel's point cloud after which the overall mean was then calculated using:

$$m\_ang_l = \frac{\left|mean\left(ang_{C_1}\right)\right| + \left|mean\left(ang_{C_2}\right)\right|}{2} \quad (3)$$

where m_ang_l is the absolute mean angle of points from flight line l; ang_{C1} and ang_{C2} are the return scan angles of the point cloud of a tree, respectively for the first and second channels of a ratio feature. The mean scan angles were always calculated from all return types of the channels that were concerned. Yet, these mean scan angles were also attributed to features that were computed only from first or single returns. These computed mean scan angles were then used (a) to calculate the Pearson product-moment correlation coefficient (r) between scan angle and feature values, (b) to divide tree views into scan angle classes, and (c) to evaluate the variation of species identification accuracy with scan angle class.

Descriptive statistics and boxplots of 3D features and intensity features that had been calculated for each channel and species were used to compare variations in feature values with mean scan angle (objective i).

We also evaluated the magnitude of the intensity normalization effect on the correlation between feature values and scan angle, and on classification accuracy (objective iv). The percentage of features that were correlated with mean scan angle with a coefficient greater than $|\pm 0.2|$ was compared between intensity features that were calculated respectively from raw and normalized intensities. To evaluate the effect of intensity normalization on species classification accuracy, results of RF classifications based upon intensity features that were calculated respectively from raw and normalized intensities were compared.

2.6. Random Forest Classification

Tree views were first divided into three classes based on their mean scan angle (Table 3). RF classifications of species were performed separately for each angular class. This method makes it possible to determine whether the mean scan angle had affected species classification accuracy (objective iii) by comparing the accuracies between the scan angle classes. The RF models were trained separately using samples that were balanced between species-scan angle class combinations to avoid bias in the RF classification. The same value was used for the *nsize* parameter of the *rf* function from the *randomForest* R library [53]. This value was set to 20 for all classifications, which was somewhat less than the sample size of the smallest tree view group of species-scan angle class. When compared to using the minimum *nsize* for each specific RF classification subset, this choice lowers the resulting accuracy for all classifications, but ensures that differences between classification accuracies cannot be attributed to differences in the *nsize* parameter settings. Note that the main objective of these classifications was not to compare performance between different types of features or channels that were used but to test whether results differed between the three scan angle classes while using the same features in the RF classification models.

Optimal delimitations were determined by creating a set comprising a small, medium and large scan angle class per channel or channel combination (Table 3). The choice of class boundaries was guided by criteria, such as ensuring that the number of trees in each group of species-scan angle class was sufficient.

Table 3. Tree views mean scan angle statistics in each channel and corresponding scan angle class boundaries used in the balanced RF classification (all values are degrees).

Channels	Min	Mean	Max	Class 1	Class 2	Class 3
C1	3.50	8.3	16.80	3–6	6–11	11–17
C2	0.02	7.17	13.00	0–5	5–10	10–15
C3	7.00	10.56	20.01	7–9	9–12	12–20
C321	2.12	8.48	16.53	2–7	7–11	11–17
C1–C2	1.78	7.69	15.38	1–5	5–10	10–16
C1–C3	5.25	9.36	17.20	5–8	8–12	12–18
C2–C3	3.53	8.83	16.16	3–7	7–11	11–17

RF classifications were performed for each individual channel and ran separately for 3D features and for intensity features (raw and normalized), together with the combined 3D and intensity features. First, for each of these RF classifications, the model was trained with all tree views from the three scan angle classes. The out-of-bag RF accuracy of this pooled classification was reported as the overall accuracy. Second, the accuracy of the RF classification for each scan angle class was then calculated separately.

3. Results

3.1. Correlation between Feature Values and Scan Angle

Our results generally show a slight influence of the mean scan angle on feature values (objective i). Moreover, feature values generally have a large variability, regardless of the scan angle. Correlations between feature values and mean scan angle, as expressed using Pearson's *r*, were generally less than $|\pm 0.2|$, with the greatest correlation being 0.55. Figure 5 provides an example of the variability of a 3D feature, the 75th percentile value of the slope between the highest point in the crown and the other first returns (3D_SL_1st_p75), with scan angle. Similarly, Figure 6 demonstrates the typical variability of an intensity feature with scan angle, the 95th percentile of intensity of the first returns (I_PE_1st_p95). We selected these two features for illustrative purposes because they were among the best features for individual tree species classification in a previous study (Budei et al., 2018) [18].

The 3D features that were most sensitive to scan angle (i.e., having correlations greater than $|\pm 0.2|$) are outlined inTable A1. Features that were related to crown shape, such as the standard deviation of slope (SL) between the highest return and the other first returns (e.g., 3D_SL_1st_sd_C1), were among the most strongly correlated (objective i). The tree species with the highest number of correlations above $|\pm 0.2|$ for SL features was *Larix laricina* (objective ii). For the features that were based upon ratios of return numbers (RP, e.g., #single returns/#1st returns, 3D_RP_si_1st_C3), *Picea abies* had the highest correlations, especially in C3 (up to 0.55). Even if correlations of percentiles of return heights with mean scan angle were very low, some trends could be observed as the angle of incidence increased. First, the percentile shift is not the same for all species. There is a downward trend for all height percentiles for *Picea abies* as scan angle increases; generally, an upward trend for *Pinus strobus*; an upward trend for *Pinus resinosa*, except for percentiles from single returns, and variable patterns for *Pinus sylvestris* and *Larix laricina* (upward for higher percentiles and downward for lower percentiles) (objective ii).

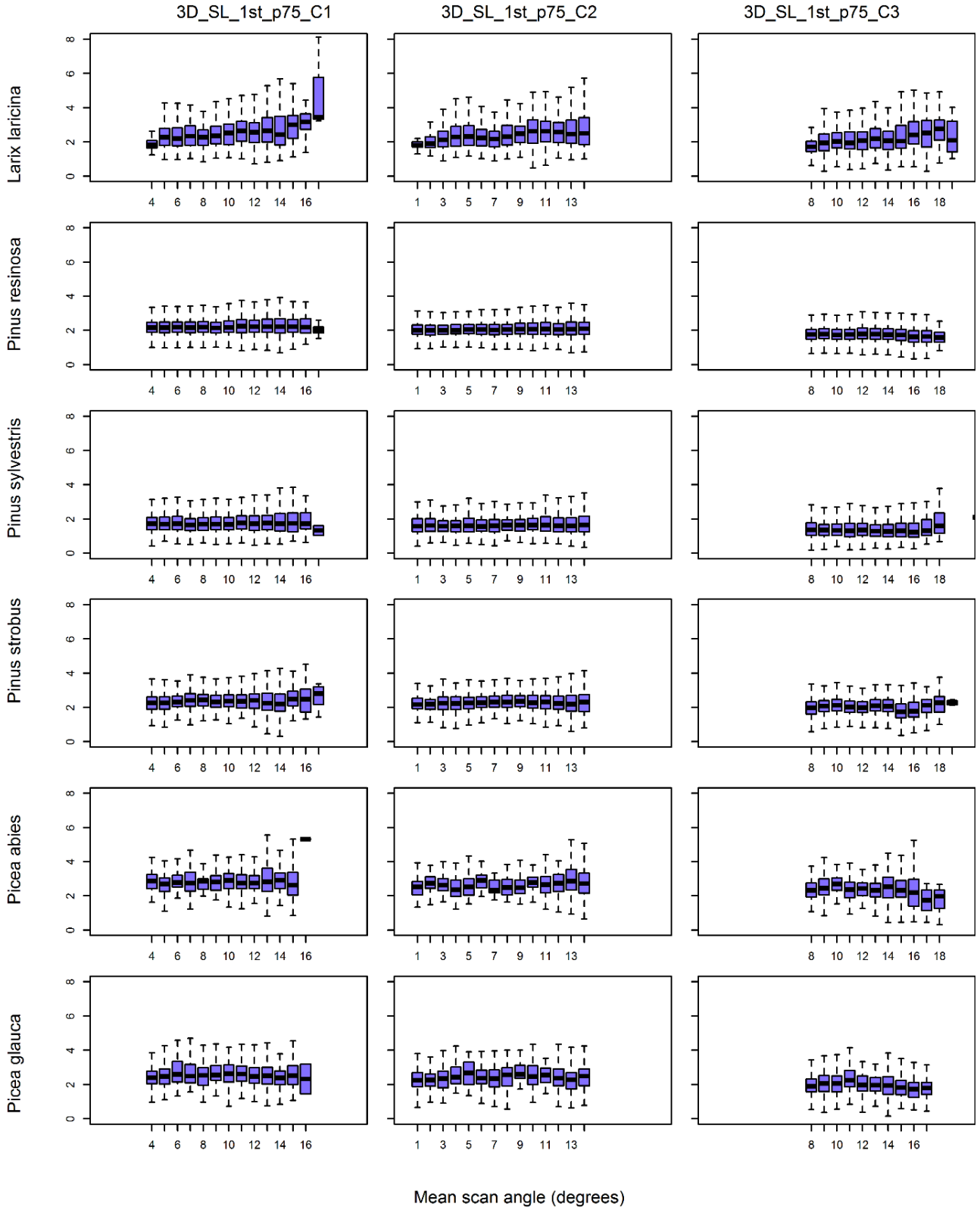

Figure 5. Variations in the feature 3D_SL_1st_p75 (75th percentile of the slope of the first returns in each of the three channels) according to scan angle, and per species.

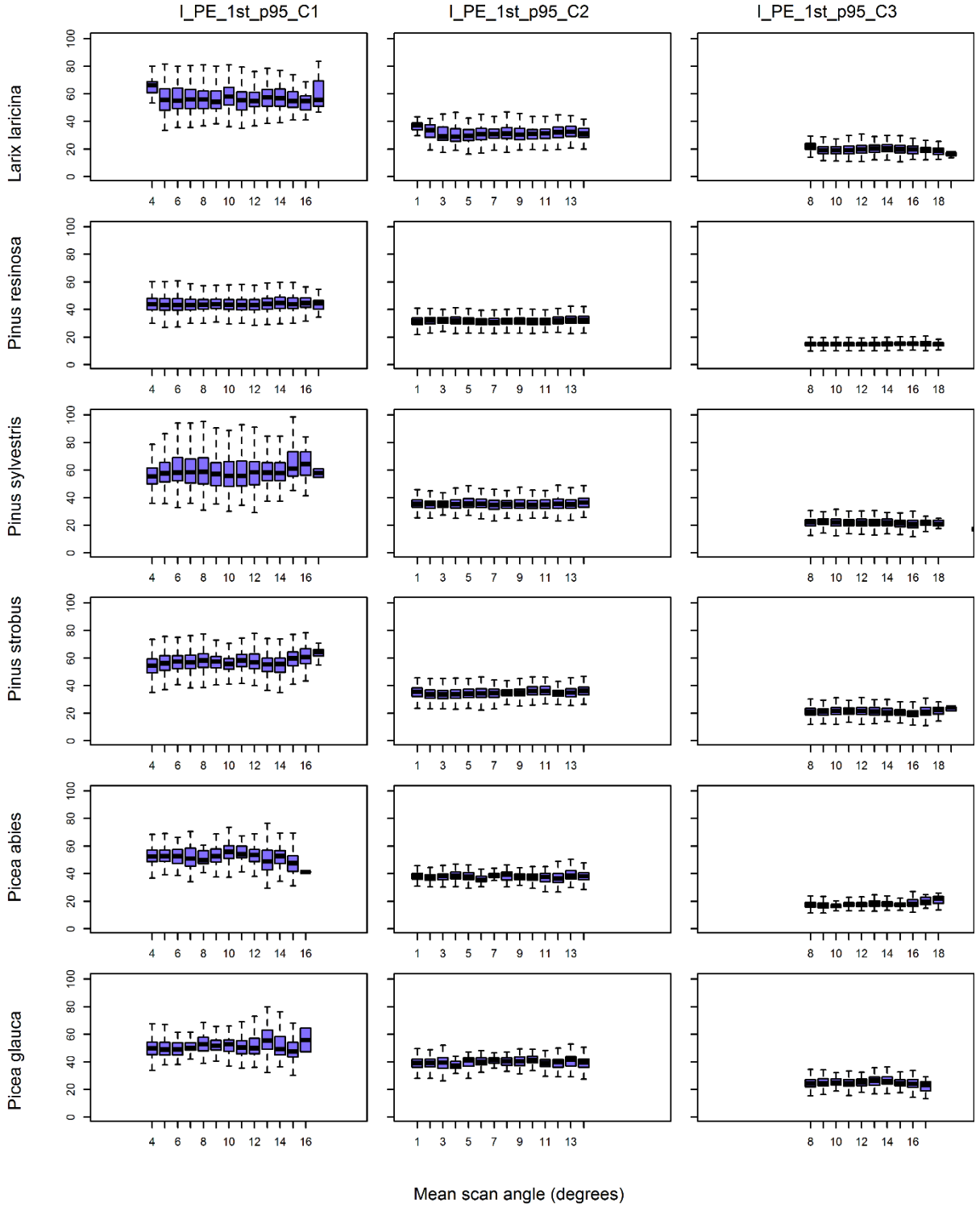

Figure 6. Variations in the feature I_PE_1st_p95 (95th percentile of the normalized intensity of the first returns in each of the three channels) according to scan angle, and per species.

The raw intensity features were the most strongly correlated with mean scan angle, and they mainly affected three species, *Picea abies*, *Picea glauca* and *Pinus sylvestris* (Table A2). Between these raw intensity features, intensity percentiles (PE), normalized mean intensities (MI) and dispersion of intensities (DI) stood out in this regard. Consistent with expectation, the intensity feature values decreased in intensity with increasing mean scan angle, eventually leading to negative correlations (objective i). Intensity normaliza-

tion reduced the feature correlation to mean scan angle (objective iv), but its beneficial impact varied among species. After intensity normalization, only intensity features for one species, *Picea abies*, remained correlated with mean scan angle (Table A3). Intensity normalization changed the values of the intensity features that were calculated on single channels and slightly decreased their variability as well as their correlation with mean scan angle (see Figure 7 for an example of the variation of an intensity feature calculated on single channels before and after normalization). In contrast, intensity features that were based upon channel ratios (RM), normalized indices (NDVIs: NDG1, NDG2, NDIR) or features describing dispersion (DI properties, such as the coefficient of variation, skewness or kurtosis) were not affected by intensity normalization. Figure 8 provides an example of NDVIs that were computed from raw and normalized intensity values as a function of scan angle. We observed a decrease in the variability of intensity features with increasing scan angle. This could be detected from the negative values in intensity dispersion features (DI), with larger negative values for *Picea abies* for both raw and normalized intensities. The intensity features in C3 had lower values and also lower variability compared to intensity features in C1 and C2. For example, note changes in the 95th intensity percentile in the three channels in Figure 6. Nevertheless, these observations do not make it possible to isolate the scan angle effect from that of wavelength and divergence differences between channels.

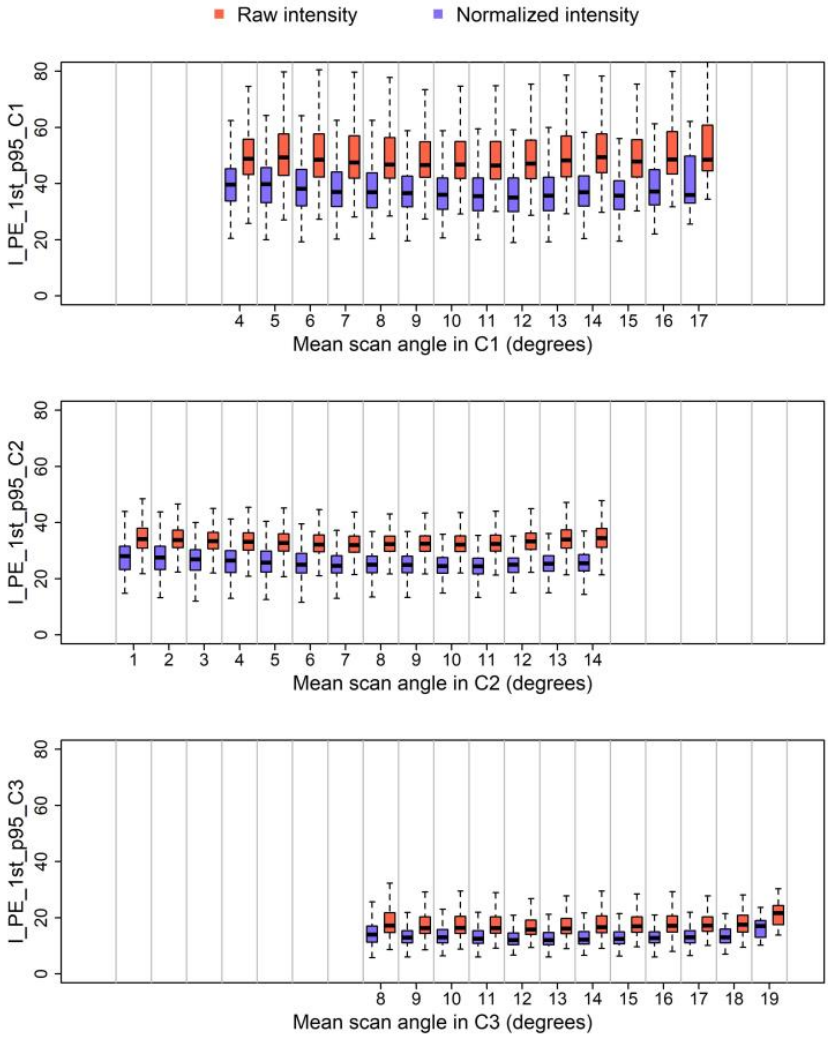

Figure 7. Raw and normalized values for the 95th percentile of intensity in the three channels as a function of mean scan angle.

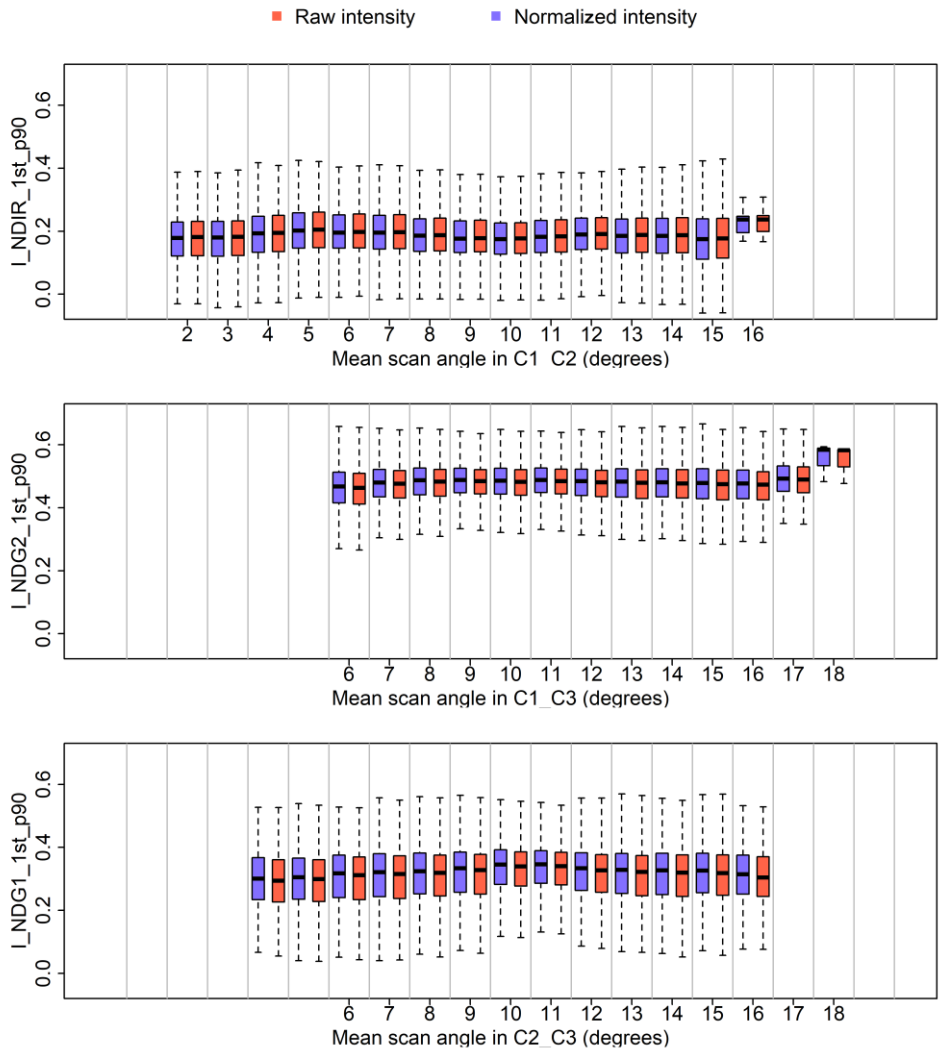

Figure 8. Normalized vegetation indices computed from raw and normalized intensity values of the 90th percentiles of first returns as a function of mean scan angle.

The detailed results that were presented in Tables A1–A3 are summarized in Tables 4 and 5. The percentage of cases having $r > |\pm 0.2|$ was calculated as:

$$Np = \frac{Nr \times 100}{Nf \times Ns} \quad (4)$$

where Nr = number of cases having $r > |\pm 0.2|$, Nf = number of features, and Ns = number of species. Table 4 presents the reduction of correlation brought about by intensity normalization (objective ii). We note that the number of cases having a correlation greater than $|\pm 0.2|$ is reduced by more than half, from 15.19%, to 6.02%, by applying intensity normalization.

Table 4. Number and percentage of cases having a correlation (r) greater than $|\pm 0.2|$ between mean scan angle and feature values.

Feature Type	Number of Features	Number of Cases Having $r > \|\pm 0.2\|$	Percent Cases Having $r > \|\pm 0.2\|$
3D	192	84	7.29%
Raw intensity	249	227	15.19%
Normalized intensity	249	90	6.02%

Table 5. Number and percentage of cases having a correlation (*r*) greater than |± 0.2| between mean scan angle and feature values by species. Cases that were greater than 15% are shaded.

	Number of Cases Having $r >$ |±0.2|			Percent Cases Having r > |±0.2|		
Species	**3D**	**Raw Intensity**	**Normalized Intensity**	**3D**	**Raw Intensity**	**Normalized Intensity**
All	5	0	0	2.60%	0.00%	0.00%
Pinus resinosa	11	0	0	5.73%	0.00%	0.00%
Pinus strobus	9	0	0	4.69%	0.00%	0.00%
Pinus sylvestris	2	56	0	1.04%	22.49%	0.00%
Picea abies	21	88	89	10.94%	35.34%	35.74%
Picea glauca	12	83	1	6.25%	33.33%	0.40%
Larix laricina	29	0	0	15.10%	0.00%	0.00%

Table 5 presents a summary of correlations between feature values and mean scan angle by species (objective ii). The species for which the 3D features varied most strongly with scan angle were *Larix laricina* and *Picea abies*, while the species for which the raw intensity features varied most with scan angle were *Picea abies*, *Picea glauca* and *Pinus sylvestris*. The species that showed a large reduction in the number of correlated intensity features following normalization were *Pinus sylvestris* and *Picea glauca*. The number of species for which there were at least two intensity features with correlations above |±0.2| between mean scan angle and single-channel intensity feature values decreased from three species to one, *Picea abies*, after normalization was applied (see Table 5). The behaviour of this species differs from the others, since there are some features for which correlation slightly increased after normalization, mainly in the case of lower intensity percentiles (5th, 10th, 25th) and features that were calculated as normalized mean intensity (MI) (see Tables A2 and A3).

Table 6 compares the percentage of features that have correlations above |±0.2| with scan angle depending upon the return type being considered (all, 1st or single returns) and species (objective i). Only features that were calculated for all three return types were considered. We see that in addition to the general decrease in percentage of correlations between raw and normalized intensity features, trends between feature types are different. For raw intensity, the most strongly correlated features were the single-return features and the least correlated were the features calculated from all returns. The opposite was observed for the normalized intensity features. This is due to the effects of a single species, i.e., *Picea abies*, which exhibits an increase in correlation for both first and all returns after normalization.

Table 6. Percent of features with a correlation (*r*) greater than |± 0.2| between mean scan angle and feature values by return type and by species. Cases that were greater than 15% are shaded.

Intensity Features	**Return Type**	***Pinus resinosa***	***Pinus strobus***	***Pinus sylvestris***	***Picea abies***	***Picea glauca***	***Larix laricina***	**All Species**
Raw	all	0.00	0.00	19.51	32.93	29.27	0.00	13.62
	1st	0.00	0.00	20.73	34.15	30.49	0.00	14.23
	si	0.00	0.00	28.05	36.59	36.59	0.00	16.87
Normalized	all	0.00	0.00	0.00	53.66	0.00	0.00	8.94
	1st	0.00	0.00	0.00	40.24	0.00	0.00	6.71
	si	0.00	0.00	0.00	10.98	1.22	0.00	2.03

3.2. Classification Accuracy

Overall accuracies for RF tree species identification are provided in Table A4. Tree species identification accuracies for each of the scan angle classes are depicted in Figure 9 with the corresponding numerical values being presented in Table A4. The accuracies

are given for different selections of features depending upon their type (3D or intensity), intensity normalization or number of channels. Changes in classification accuracy between scan angle classes were small. Generally, no clear or systematic decrease in classification accuracies was evident with increasing scan angle (objective iii). The intermediate scan angle class sometimes yielded slightly better results than the others. Even if the classification accuracies for individual feature groups were low, our main interest lies in understanding how classification accuracy in each feature group varies with scan angle class and how it subsequently may influence overall accuracy (resulting from all scan angle classes or all features). The number of tree views in a class varies according to features that are used in classification because the division of tree views into scan angle classes is calculated for each specific channel or subset of channels that are used in the features. Yet, even if classification accuracies may be influenced by the variation in the number of tree views in each class, we consider that the large number of tree views in each scan angle class permits comparisons between corresponding scan angle classes, without significant error.

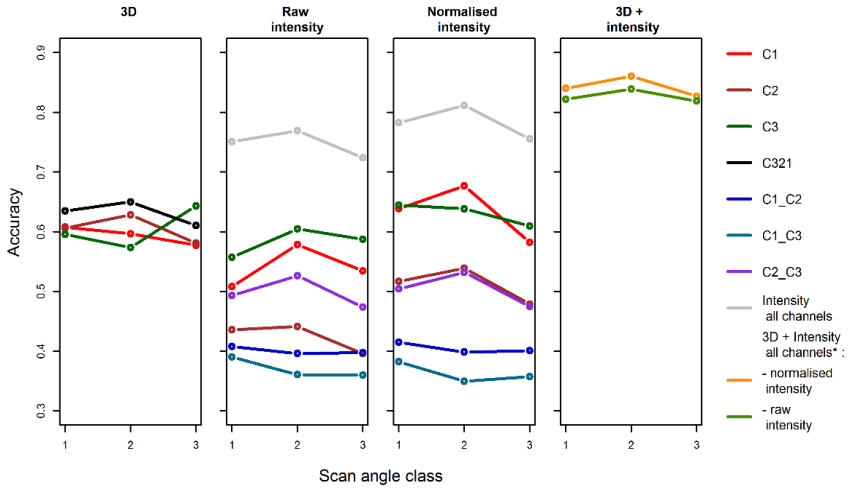

Figure 9. Random forest species identification accuracy by scan angle class. * Channels used in "3D + intensity" are C321 for 3D and C1, C2, C3, C1_C2, C1_C3, C2_C3 for intensity.

In the case of classifications using only single channel 3D features, there was a difference in accuracy variations between the scan angle classes of the three channels. There was no systematic decrease in accuracy from the first class (near vertical) to the third class (oblique). Accuracy in the first scan angle class was very similar between channels, it varied by only 1%. However, accuracy varied by 6% for the two other scan angle classes. Surprisingly, the best accuracy that was obtained from single channel 3D features was in C3 in the large scan angle class. The accuracy that was obtained from 3D features from C321 was generally slightly higher (by 3–5%) than the accuracy that was obtained from single channel 3D features, with the higher accuracy for the second class. In the case of intensity features, all accuracies that were obtained with single channel normalized intensity were higher than their raw intensity counterparts, with an improvement between 5% and 10%. The accuracy of all two-channel combinations remained almost the same after normalization, i.e., variations of $\pm$1% (Table 7). In general, the accuracy of the second scan angle class was the highest. Conversely, the lowest accuracy was in the first scan angle class with raw intensities of C1 and C3. For almost all intensity features groups, accuracy decreased from Class 2 to Class 3. Once the intensities were normalized, the lowest accuracy was seen in the third scan angle class. The highest accuracies were achieved when combining all features (3D plus intensity); more so when the 3D features were combined with the normalized intensity (objective iv). In this case, accuracy variations with scan angle class were very weak (3%). Within this weak margin, the highest variations were recorded in the intermediate scan angle class. A summary of classification accuracy improvement after intensity normalization is given in Table 7.

Table 7. Improvement in accuracy between classifications using normalized intensity features compared to classifications using raw intensity features. Results are presented as overall (second column) and by mean scan angle class (columns 3–5), for classifications with different feature selection (rows). Cases that were improved by ≥0.10 are highlighted in grey.

Features	Overall Accuracy Improvement	Accuracy Improvement in Angle Class 1	Accuracy Improvement in Angle Class 2	Accuracy Improvement in Angle Class 3
C1	0.10	0.13	0.10	0.05
C2	0.09	0.08	0.10	0.08
C3	0.06	0.08	0.04	0.02
Mean single channel	0.08	0.10	0.08	0.05
C1–C2	0.00	0.01	0.00	0.00
C1–C3	0.00	−0.01	−0.01	0.00
C2–C3	0.01	0.01	0.00	0.00
Mean channel ratios	0.00	0.00	0.00	0.00
all intensity	0.04	0.03	0.04	0.04
3D + intensity	0.02	0.02	0.02	0.01

4. Discussion

The scan angle of airborne laser scanners is variable and can theoretically affect the 3D distribution and intensity of returns from tree crowns. This could affect our capacity to use lidar point clouds to identify individual tree species, but research on this question was lacking. This study on individual trees, which was similar to plot-level studies, showed that for net scan angles between 0° and 20° and over terrain having only small topographic variations, the correlation between individual tree feature values and scan angle was low, i.e., generally less than $|\pm 0.2|$ (objective i). At the same time, variability in individual tree feature values for a given tree species that had been captured from about the same scan angles (see boxplots in Figures 5–8) was itself quite large. The inherently large feature variability dampens our ability to isolate the relative effect of scan angle. A similar situation was observed for plot-level features. For example, Morsdorf [45] found that there was not a significant difference between the predicted percent canopy cover at larger scan angles than at lower scan angles because their inherent standard deviations were larger than the differences. This large variability might be explained by other tree properties; for example, Budei and St-Onge [18] highlighted the influence of tree height on feature values and [44] highlighted the influence of tree density on feature values. Even considering the controlled conditions of our test site, the effect of scan angle on feature values did not predominate over feature variability.

Our analysis highlighted several effects that were attributable to scan angles (objective i). The features that were most affected by scan angle were those related to crown shape, return proportions and single-channel intensity. Effect #2 of scan angle (decrease in the number of returns per emitted pulse) explains the higher correlations of features, such as the return proportion (RP), because the number of second- and third-returns are reduced as scan angle increases. In addition, features that are related to crown shape (SL and SU) are highly sensitive to return distributions in the crown, being equally influenced by scan angle effects #2 and #3 (change in the distribution of returns) (Table A1). The single-channel intensity features that were computed from first- or single-returns were related mainly to effect #1 (intensity attenuation), compared to those computed from all returns; the latter are influenced equally by effects #1 and #2. Thus, range normalization generally reduced correlations with scan angle for intensity features from first- and single-returns, and had less importance with respect to features that were computed from all returns (Table 6).

The features that were least sensitive to scan angle are NDVIs and intensity channel ratios. The reason is likely that scan angle effects #1 and #2 more or less offset one another in

the case of ratios between channels. Yet, configuration differences between Titan channels must be accounted for when considering the ratios of channels and NDVIs. Overall, our analysis shows that the effect of scan angle on channel ratios and NDVIs can be ignored for scan angles lower than 15°.

The influence of tree species on the variation lidar features (objective ii), i.e., the different upward or downward shifts in height percentile depended on tree species. For example, features that are calculated for species with an elongated tree crown length, (e.g., spruces) were more affected by scan angle than those calculated for species with shorter crown lengths and more compact crown shapes (e.g., pines). This observation was consistent with simulation studies, such as the one conducted by [44].

Our assessment of an alternative solution to circumvent normalization showed that classification improvement following intensity normalization depends upon the percentage of features that are affected by intensity normalization. Intensity normalization changed feature values that were calculated from single channels, such as percentiles of intensity. Intensity normalization did not substantially change the feature values that were calculated as ratios of channels, NDVIs or dispersion characteristics. Consequently, features such as ratios, NDVIs or 3D reduce the necessity of intensity normalization for tree species identification compared to using intensity features from a single channel. The possibility of reducing the necessity of intensity normalization by using features that were computed from two channels is a major advantage of multispectral lidar compared to mono-spectral lidar.

At least two limitations remain in our study and need further assessment. The first limitation concerns the exclusion of trees at large scan angles. For single trees, occlusions occurring at large scan angles can lead to the impossibility of calculating all features for a given tree. The uneven point spacing at swath ends or at low-return density (in this study a single flight line) may also lead to the impossibility of calculating all features; a concern that especially applies to smaller trees. This study being limited to trees above 10 m high, the overall ability to identify species of smaller trees at large scan angle is worth considering in further studies, as errors are expected to increase. The second limitation concerns the progressive importance of occlusion effects and interception as scan angles become larger, which in turn influences the variability and the correlation of feature values with scan angle. These effects would also be increased by greater variations in topography [30]. For large scan angles, occlusions that were incurred by taller trees or through self-occlusion cause lateral asymmetry of return distribution in the crown.

The data that were used in this study were registered with a maximum lateral scan angle of 15°, which resulted in a net scan angle up to 20°. Further studies would be needed to verify the effect of larger scan angles (e.g., up to 30°).

The methods that were used in this study isolated the individual flight lines, an approach that allows clear division of trees into scan angle classes, given that all pulses that reach a tree view had similar scan angles. In most cases, airborne lidar flight lines are laid out such that scanning swaths from at least two flight lines overlap. This reduces occlusions and mitigates scan angle effects. However, survey costs increase with the percentage of swath overlap, creating a situation where a compromise must be sought between accuracy and costs.

5. Conclusions

The objective of the present study was to evaluate whether scan angle (up to a net scan angle of 20°) influences 3D and intensity feature values and if this influence affected species classification accuracy. Quantifying the magnitude of this influence is important from an operational perspective, especially in choosing the best scanning parameters when species identification is considered. In the context of our study, we found that:

1. Scan angle had a small effect on 3D feature values. Yet, this influence differed depending upon tree species, with *Picea abies* and *Larix laricina* having the greatest number of correlated features above $|\pm 0.2|$.

2. Scan angle had a greater effect on raw (non-normalized) intensity feature values (mostly concerning *Picea abies*, *Picea glauca* and *Pinus sylvestris*) than on normalized ones (when only one species being concerned, i.e., *Picea abies*). Yet, this effect almost disappeared when channel ratios or normalized vegetation indices (NDVIs) were used, these features being the least correlated with scan angle.
3. Classification accuracy did not vary with scan angle when 3D features and the best intensity features (the ones that were least affected by scan angle) were used together.

Despite theoretical expectations that scan angle might affect 3D or intensity features and, consequently, species identification accuracy, this study highlights the fact that the magnitude of the effect is small and can be mitigated. Mitigation can be accomplished by combining plot clouds from multiple overlapping flight lines by standardizing the intensity channel if only one exists, or by using ratios or normalized differences of intensity if at least two channels (wavelengths) are available. Furthermore, by selecting the 3D and intensity features that are least sensitive to scan angle, as identified in our study, the scan angle effect can be ignored. This potentially alleviates the necessity of applying complex methods that compensate for scan angle effects. If these precautions are not taken, errors in tree species identification could vary, to a certain extent, as a function of scan angle, thereby, generating false spatial patterns of species distributions.

Author Contributions: Conceptualization, B.C.B. and B.S.-O.; methodology, B.C.B., B.S.-O., R.A.F. and D.K.; software, B.C.B.; validation, B.C.B.; formal analysis, B.C.B.; investigation, B.C.B.; resources, B.S.-O. and D.K.; data curation, B.C.B.; writing—original draft preparation, B.C.B.; writing—review and editing, B.C.B., B.S.-O., R.A.F. and D.K.; visualization, B.C.B.; supervision, B.S.-O., R.A.F. and D.K.; project administration, B.S.-O., B.C.B. and D.K.; funding acquisition, B.S.-O., R.A.F. and D.K. All authors have read and agreed to the published version of the manuscript.

Funding: This study was partly funded by the Natural Sciences and Engineering Research Council of Canada, by the AWARE project (NSERC File: CRDPJ 462973-14, Grantee: N.C. Coops, FRM, UBC), in collaboration with Canadian Wood Fiber Centre (CWFC), FP-Innovations.

Acknowledgments: We express our thanks to Teledyne Optech Inc. (Vaughan, ON, Canada) for graciously providing the Titan MSL datasets used in this study. We thank authorities of the York Regional Forest (Kevin Reese) for granting permission and facilitating access to the forest's study area. We acknowledge the collaboration of CarboMap (Edinburgh, Scotland) in field logistics and data collection. Chris Hopkinson provided us with field measurements. W.F.J. Parsons edited the English text.

Conflicts of Interest: The authors declare no conflict of interest.

Appendix A

Table A1. Correlations (*r*) between 3D features and mean scan angle.

Feature *	All Trees	*Pinus resinosa*	*Pinus strobus*	*Pinus sylvestris*	*Picea abies*	*Picea glauca*	*Larix laricina*	Count of Correlations ≥0.2 or <−0.2
3D_DI_all_cv_C1	0.03	0.03	0.00	0.02	0.04	0.00	**0.22**	1
3D_DI_all_cv_C2	0.02	0.01	−0.02	0.03	0.08	0.06	0.15	0
3D_DI_all_cv_C3	−0.03	−0.06	−0.05	−0.03	−0.01	−0.05	0.12	0
3D_DI_all_sd_C1	0.04	0.04	0.00	0.02	0.03	0.00	**0.21**	1
3D_DI_all_sd_C2	0.03	0.02	−0.02	0.03	0.06	0.07	0.15	0
3D_DI_all_sd_C3	−0.03	−0.06	−0.05	−0.03	−0.03	−0.05	0.11	0
3D_HR_all_cv_C1	−0.14	−0.16	−0.18	−0.06	−0.10	−0.16	−0.08	0
3D_HR_all_cv_C2	−0.17	**−0.20**	−0.16	−0.14	−0.11	−0.11	−0.12	1
3D_HR_all_cv_C3	−0.03	−0.06	−0.08	0.03	−0.05	−0.04	0.06	0
3D_HR_all_lm_C1	0.19	**0.23**	**0.22**	0.12	**0.24**	**0.22**	0.14	4
3D_HR_all_lm_C2	**0.21**	**0.25**	0.19	**0.20**	**0.25**	**0.23**	0.14	5

Table A1. *Cont.*

Feature *	All Trees	*Pinus resinosa*	*Pinus strobus*	*Pinus sylvestris*	*Picea abies*	*Picea glauca*	*Larix laricina*	Count of Correlations ≥0.2 or <−0.2
3D_HR_all_lm_C3	0.04	0.09	0.10	0.02	**0.22**	0.06	−0.08	1
3D_MH_si_mn_C1	0.00	−0.03	0.02	−0.05	**−0.21**	−0.01	−0.08	1
3D_MH_si_mn_C2	0.01	−0.02	0.02	−0.05	**−0.21**	−0.04	−0.12	1
3D_MH_si_mn_C3	−0.01	−0.01	0.02	−0.04	−0.14	0.01	−0.18	0
3D_PE_all_p05_C1	−0.03	−0.04	0.00	0.00	−0.04	0.00	**−0.20**	1
3D_PE_all_p05_C2	−0.01	0.00	0.02	−0.01	−0.07	−0.06	−0.12	0
3D_PE_all_p05_C3	0.04	0.06	0.05	0.04	0.00	0.05	−0.11	0
3D_PE_si_p25_C1	−0.01	−0.02	0.02	−0.07	**−0.21**	−0.03	−0.09	1
3D_PE_si_p25_C2	0.01	−0.01	0.02	−0.07	−0.18	−0.05	−0.11	0
3D_PE_si_p25_C3	−0.02	−0.02	0.02	−0.04	−0.10	−0.02	−0.19	0
3D_PE_si_p50_C1	0.00	−0.03	0.01	−0.04	**−0.21**	0.01	−0.07	1
3D_PE_si_p50_C2	0.02	−0.02	0.02	−0.02	**−0.20**	−0.01	−0.08	1
3D_PE_si_p50_C3	−0.01	−0.03	0.02	−0.03	−0.16	0.04	−0.17	0
3D_RB_all_pt_0_60_C1	0.04	0.03	0.01	0.02	0.09	0.01	**0.22**	1
3D_RB_all_pt_0_60_C2	0.03	0.02	0.00	0.03	0.11	0.07	0.16	0
3D_RB_all_pt_0_60_C3	0.00	−0.04	−0.01	−0.01	0.06	0.00	0.12	0
3D_RM_1st_mn_all_mn_C1	0.02	0.02	0.02	−0.03	−0.16	−0.05	0.17	0
3D_RM_1st_mn_all_mn_C2	0.01	−0.01	−0.02	−0.04	−0.07	−0.01	0.13	0
3D_RM_1st_mn_all_mn_C3	−0.11	−0.12	−0.09	−0.13	**−0.21**	−0.17	0.00	1
3D_RP_1st_all_C1	0.00	−0.02	0.00	0.05	**0.39**	0.05	−0.11	1
3D_RP_1st_all_C2	0.02	0.01	0.05	0.06	**0.36**	0.02	−0.12	1
3D_RP_1st_all_C3	0.16	0.14	0.06	0.18	**0.52**	**0.22**	0.03	2
3D_RP_si_1st_C1	0.07	0.09	0.08	0.08	**0.40**	0.08	0.06	1
3D_RP_si_1st_C2	0.06	0.07	0.10	0.09	**0.40**	0.08	0.09	1
3D_RP_si_1st_C3	**0.21**	**0.22**	0.09	**0.23**	**0.55**	**0.25**	0.13	5
3D_SL_1st_cv_C1	0.18	**0.20**	**0.21**	0.13	**0.20**	**0.24**	0.20	4
3D_SL_1st_cv_C2	0.19	0.19	**0.25**	0.16	**0.23**	**0.25**	**0.20**	4
3D_SL_1st_cv_C3	0.05	0.05	0.07	0.03	0.14	0.06	0.07	0
3D_SL_1st_mn_C1	0.13	0.14	0.13	0.09	0.11	0.11	**0.24**	1
3D_SL_1st_mn_C2	0.11	0.12	0.13	0.12	0.17	0.11	**0.21**	1
3D_SL_1st_mn_C3	0.02	0.00	0.02	0.02	−0.05	−0.06	**0.25**	1
3D_SL_1st_p75_C1	0.09	0.09	0.07	0.06	0.08	0.07	**0.24**	1
3D_SL_1st_p75_C2	0.08	0.07	0.07	0.08	0.14	0.09	**0.21**	1
3D_SL_1st_p75_C3	0.02	−0.01	0.00	0.02	−0.04	−0.05	**0.25**	1
3D_SL_1st_sd_C1	0.19	**0.21**	**0.23**	0.12	**0.21**	**0.26**	**0.26**	5
3D_SL_1st_sd_C2	0.18	0.18	**0.22**	0.16	**0.23**	**0.21**	**0.28**	4
3D_SL_1st_sd_C3	0.05	0.04	0.08	0.03	0.05	0.01	**0.21**	1
3D_SL_all_cv_C1	0.20	**0.21**	**0.22**	0.10	0.15	**0.23**	**0.27**	4
3D_SL_all_cv_C2	**0.26**	**0.29**	**0.26**	0.19	**0.24**	**0.32**	**0.23**	6
3D_SL_all_cv_C3	0.04	0.03	0.07	0.03	0.14	0.03	0.06	0
3D_SL_all_mn_C1	0.19	**0.20**	0.16	0.11	0.04	0.13	**0.34**	2
3D_SL_all_mn_C2	0.19	0.20	0.17	0.15	0.14	0.18	**0.28**	1
3D_SL_all_mn_C3	−0.02	−0.05	0.01	−0.02	−0.13	−0.13	**0.25**	1
3D_SL_all_p50_C1	0.04	0.03	−0.01	0.02	−0.07	−0.01	**0.21**	1
3D_SL_all_p50_C2	0.01	0.00	−0.01	0.02	−0.05	−0.01	0.16	0
3D_SL_all_p50_C3	−0.05	−0.08	−0.04	−0.03	−0.17	−0.13	**0.21**	1
3D_SL_all_p75_C1	0.13	0.13	0.11	0.08	−0.01	0.08	**0.29**	1
3D_SL_all_p75_C2	0.10	0.08	0.08	0.09	0.07	0.10	**0.25**	1
3D_SL_all_p75_C3	−0.02	−0.06	−0.02	−0.03	−0.12	−0.11	**0.25**	1
3D_SL_all_sd_C1	**0.21**	**0.21**	**0.22**	0.12	0.12	**0.23**	**0.35**	5
3D_SL_all_sd_C2	**0.25**	**0.26**	**0.24**	0.20	**0.23**	**0.28**	**0.29**	6
3D_SL_all_sd_C3	0.02	0.00	0.07	0.02	−0.02	−0.07	0.20	0
3D_SU_1st_rs_C1	0.04	0.02	0.01	0.06	0.11	0.10	**0.26**	1
3D_SU_1st_rs_C2	0.05	0.02	0.01	0.11	0.16	0.14	**0.21**	1
3D_SU_1st_rs_C3	−0.02	−0.05	−0.03	0.00	0.01	0.00	**0.21**	1
Count of correlations ≥0.2 or >−0.2	5	11	9	2	21	12	29	84

* 3D features that did not have at least one correlation value larger than |±0.2| with the mean scan angle in any of the three channels and for any species were not presented in this table, but are listed here: AH, DI_1st_cv, DI_1st_kurt, DI_1st_sd, DI_1st_skew, DI_all_kurt, DI_all_skew, DI_si_kurt, DI_si_sd, DI_si_skew, HR_si_cv, HR_si_lm, MH_1st_mn, MH_all_mn, PE_1st_p05, PE_1st_p10, PE_1st_p25, PE_1st_p50, PE_1st_p75, PE_1st_p90, PE_1st_p95, PE_all_p10, PE_all_p25, PE_all_p50, PE_all_p75, PE_all_p90, PE_all_p95, PE_si_p50, RB_all_pt_60_80, RB_all_pt_80_90, RB_all_pt_90_100, RB_all_pt_95_100, RM_1st_mn, RM_1st_p50_1st_mn, RM_1st_p50, RM_all_mn, RM_all_p50_all_mn, RM_all_p50, SL_1st_p25, SL_1st_p50, SL_all_p25, SU_1st_coef. The description of feature names is given in Table 2. Correlations values higher than |±0.2| are highlighted in boldface type.

Table A2. Correlations between raw intensity features and mean scan angle.

Feature *	All Trees	*Pinus resinosa*	*Pinus strobus*	*Pinus sylvestris*	*Picea abies*	*Picea glauca*	*Larix laricina*	Count of Correlations ≥0.2 or <−0.2
I_DI_1st_cv_C1	−0.05	−0.04	−0.05	−0.02	**−0.33**	−0.04	−0.02	1
I_DI_1st_cv_C2	−0.01	−0.02	−0.03	0.04	**−0.21**	0.02	0.03	1
I_DI_1st_cv_C3	−0.08	−0.06	−0.04	−0.09	**−0.37**	−0.08	−0.02	1
I_DI_1st_sd_C1	−0.11	−0.10	0.03	−0.14	**−0.49**	**−0.26**	0.05	2
I_DI_1st_sd_C2	−0.12	−0.10	0.04	−0.18	**−0.44**	**−0.31**	0.14	2
I_DI_1st_sd_C3	−0.13	−0.12	0.00	**−0.28**	**−0.29**	**−0.30**	0.00	3
I_DI_1st_skew_C1	−0.05	−0.05	−0.10	−0.02	**−0.26**	−0.07	−0.03	1
I_DI_1st_skew_C2	−0.02	−0.01	−0.08	0.02	**−0.21**	−0.02	0.01	1
I_DI_1st_skew_C3	−0.07	−0.06	−0.09	−0.05	**−0.24**	−0.04	−0.05	1
I_DI_all_cv_C1	−0.05	−0.05	−0.02	−0.05	**−0.39**	−0.05	−0.02	1
I_DI_all_cv_C2	0.01	0.01	0.00	0.00	**−0.34**	0.04	0.07	1
I_DI_all_cv_C3	−0.09	−0.07	−0.01	−0.12	**−0.38**	−0.09	−0.01	1
I_DI_all_sd_C1	−0.12	−0.12	0.05	−0.16	**−0.49**	**−0.30**	0.04	2
I_DI_all_sd_C2	−0.13	−0.11	0.06	**−0.23**	**−0.37**	**−0.36**	0.13	3
I_DI_all_sd_C3	−0.12	−0.13	0.02	**−0.28**	**−0.23**	**−0.30**	0.01	3
I_DI_all_skew_C1	−0.03	−0.03	−0.07	−0.02	**−0.31**	−0.04	0.01	1
I_DI_all_skew_C2	0.00	0.00	−0.07	0.00	**−0.33**	0.04	0.05	1
I_DI_all_skew_C3	−0.09	−0.07	−0.10	−0.10	**−0.30**	−0.07	−0.07	1
I_DI_si_sd_C1	−0.08	−0.06	−0.06	−0.06	**−0.32**	−0.20	0.03	1
I_DI_si_sd_C2	−0.07	−0.05	−0.02	−0.09	−0.16	−0.18	0.17	0
I_DI_si_sd_C3	−0.09	−0.08	0.00	**−0.21**	**−0.33**	−0.16	0.08	2
I_IR_all_sd_C1	−0.07	−0.10	0.06	−0.05	−0.12	**−0.20**	−0.06	1
I_IR_all_sd_C2	−0.09	−0.10	0.03	−0.11	−0.05	**−0.23**	−0.05	1
I_IR_all_sd_C3	−0.06	−0.07	0.04	−0.14	−0.05	**−0.22**	−0.04	1
I_IR_si_sd_C1	−0.03	−0.05	0.05	−0.04	−0.13	−0.16	0.02	0
I_IR_si_sd_C2	−0.03	−0.04	0.04	−0.04	−0.01	−0.19	0.03	0
I_IR_si_sd_C3	−0.06	−0.07	0.04	−0.14	−0.09	**−0.22**	−0.02	1
I_MI_1st_10_90_mn_C1	−0.10	−0.12	0.10	−0.20	**−0.22**	**−0.31**	0.09	2
I_MI_1st_10_90_mn_C2	−0.11	−0.10	0.08	**−0.24**	−0.07	**−0.34**	0.13	2
I_MI_1st_10_90_mn_C3	−0.10	−0.09	0.06	**−0.29**	0.10	**−0.28**	0.06	2
I_MI_1st_5_95_mn_C1	−0.11	−0.12	0.10	−0.20	**−0.24**	**−0.32**	0.09	2
I_MI_1st_5_95_mn_C2	−0.11	−0.10	0.08	**−0.24**	−0.08	**−0.35**	0.13	2
I_MI_1st_5_95_mn_C3	−0.11	−0.09	0.05	**−0.30**	0.08	**−0.29**	0.05	2
I_MI_1st_mn_C1	−0.11	−0.13	0.09	−0.20	**−0.28**	**−0.34**	0.09	2
I_MI_1st_mn_C2	−0.12	−0.10	0.07	**−0.25**	−0.10	**−0.36**	0.14	2
I_MI_1st_mn_C3	−0.11	−0.10	0.04	**−0.32**	0.07	**−0.31**	0.05	2
I_MI_all_10_90_mn_C1	−0.11	−0.13	0.08	−0.18	−0.08	**−0.28**	0.08	1
I_MI_all_10_90_mn_C2	−0.11	−0.10	0.07	**−0.20**	0.07	**−0.32**	0.11	2
I_MI_all_10_90_mn_C3	−0.08	−0.06	0.05	**−0.26**	0.15	**−0.24**	0.08	2
I_MI_all_10_90_n_mn_C1	0.04	0.04	0.05	0.04	**0.25**	0.09	0.00	1
I_MI_all_10_90_n_mn_C2	0.02	0.02	0.03	0.04	**0.23**	0.02	−0.06	1
I_MI_all_10_90_n_mn_C3	0.07	0.05	0.04	0.10	0.13	0.10	0.06	0
I_MI_all_5_95_mn_C1	−0.11	−0.13	0.08	−0.18	−0.11	**−0.30**	0.08	1
I_MI_all_5_95_mn_C2	−0.11	−0.10	0.07	**−0.21**	0.05	**−0.33**	0.11	2
I_MI_all_5_95_mn_C3	−0.09	−0.07	0.05	**−0.27**	0.14	**−0.25**	0.07	2
I_MI_all_5_95_n_mn_C1	0.03	0.03	0.03	0.05	**0.20**	0.08	−0.04	1
I_MI_all_5_95_n_mn_C2	0.02	0.02	0.02	0.03	0.19	0.04	−0.05	0
I_MI_all_5_95_n_mn_C3	0.07	0.05	0.03	0.10	0.13	0.07	0.04	0
I_MI_all_mn_C1	−0.12	−0.14	0.08	−0.19	−0.16	**−0.33**	0.08	1
I_MI_all_mn_C2	−0.12	−0.11	0.07	**−0.22**	0.02	**−0.35**	0.12	2
I_MI_all_mn_C3	−0.10	−0.08	0.05	**−0.29**	0.12	**−0.27**	0.07	2
I_MI_si_10_90_mn_C1	−0.11	−0.11	0.10	−0.19	**−0.53**	**−0.32**	0.06	2
I_MI_si_10_90_mn_C2	−0.14	−0.11	0.05	**−0.27**	**−0.50**	**−0.43**	0.11	3
I_MI_si_10_90_mn_C3	−0.16	−0.16	0.01	**−0.35**	−0.11	**−0.40**	−0.03	2
I_MI_si_5_95_mn_C1	−0.11	−0.11	0.09	−0.18	**−0.53**	**−0.33**	0.06	2
I_MI_si_5_95_mn_C2	−0.14	−0.11	0.05	**−0.27**	**−0.51**	**−0.44**	0.11	3
I_MI_si_5_95_mn_C3	−0.16	−0.16	0.01	**−0.35**	−0.11	**−0.41**	−0.04	2
I_MI_si_mn_C1	−0.11	−0.12	0.09	−0.19	**−0.54**	**−0.35**	0.06	2
I_MI_si_mn_C2	−0.14	−0.12	0.05	**−0.27**	**−0.52**	**−0.46**	0.12	3
I_MI_si_mn_C3	−0.17	−0.17	0.00	**−0.37**	−0.13	**−0.42**	−0.04	2
I_NDG2_1st_mn	0.03	−0.02	0.08	0.04	**−0.21**	0.04	0.02	1
I_NDG2_1st_p50	0.02	−0.03	0.07	0.02	−0.15	0.04	0.01	0
I_NDG2_1st_p75	0.03	−0.02	0.08	0.05	**−0.22**	0.04	0.00	1

Table A2. *Cont.*

Feature *	All Trees	*Pinus resinosa*	*Pinus strobus*	*Pinus sylvestris*	*Picea abies*	*Picea glauca*	*Larix laricina*	Count of Correlations ≥0.2 or <−0.2
I_NDG2_1st_p90	0.04	−0.01	0.08	0.06	**−0.23**	0.03	0.00	1
I_NDG2_1st_p95	0.04	−0.01	0.07	0.06	**−0.21**	0.03	0.02	1
I_NDG2_all_mn	0.00	−0.05	0.07	0.02	−0.20	0.00	0.00	0
I_NDG2_all_p50	−0.01	−0.04	0.05	0.00	−0.09	0.01	−0.03	0
I_NDG2_all_p75	0.01	−0.05	0.07	0.02	−0.20	0.01	−0.02	0
I_NDG2_all_p90	0.02	−0.04	0.08	0.05	**−0.24**	0.02	−0.04	1
I_NDG2_all_p95	0.03	−0.03	0.06	0.05	**−0.22**	0.02	0.01	1
I_NDG2_si_mn	0.09	0.04	0.12	0.12	**−0.22**	0.16	0.09	1
I_NDG2_si_p50	0.09	0.04	0.10	0.11	**−0.21**	0.17	0.08	1
I_NDG2_si_p75	0.07	0.02	0.09	0.09	**−0.21**	0.11	0.02	1
I_NDG2_si_p90	0.06	0.01	0.07	0.09	−0.18	0.08	0.03	0
I_NDG2_si_p95	0.06	0.01	0.07	0.08	−0.16	0.07	0.03	0
I_PE_1st_p05_C1	−0.04	−0.04	0.01	−0.08	0.12	−0.14	0.08	0
I_PE_1st_p05_C2	−0.04	−0.03	−0.01	−0.11	0.09	−0.15	0.05	0
I_PE_1st_p05_C3	−0.05	−0.04	0.01	−0.16	**0.22**	−0.15	0.07	1
I_PE_1st_p10_C1	−0.04	−0.04	0.03	−0.09	0.15	−0.14	0.08	0
I_PE_1st_p10_C2	−0.04	−0.03	0.01	−0.13	0.12	−0.15	0.07	0
I_PE_1st_p10_C3	−0.06	−0.05	0.01	−0.18	**0.23**	−0.16	0.09	1
I_PE_1st_p25_C1	−0.06	−0.06	0.07	−0.13	0.11	−0.19	0.08	0
I_PE_1st_p25_C2	−0.06	−0.05	0.05	−0.17	0.09	−0.19	0.10	0
I_PE_1st_p25_C3	−0.08	−0.06	0.03	**−0.23**	0.18	**−0.21**	0.06	2
I_PE_1st_p50_C1	−0.10	−0.12	0.10	−0.20	−0.14	**−0.27**	0.08	1
I_PE_1st_p50_C2	−0.10	−0.09	0.08	**−0.22**	−0.01	**−0.31**	0.11	2
I_PE_1st_p50_C3	−0.10	−0.08	0.06	**−0.27**	0.10	**−0.25**	0.05	2
I_PE_1st_p75_C1	−0.11	−0.13	0.10	**−0.21**	**−0.39**	**−0.33**	0.08	3
I_PE_1st_p75_C2	−0.13	−0.11	0.08	**−0.26**	**−0.22**	**−0.40**	0.12	3
I_PE_1st_p75_C3	−0.11	−0.10	0.05	**−0.30**	0.01	**−0.29**	0.04	2
I_PE_1st_p90_C1	−0.11	−0.11	0.07	−0.16	−0.46	**−0.34**	0.08	2
I_PE_1st_p90_C2	−0.13	−0.11	0.06	−0.24	−0.33	**−0.41**	0.14	3
I_PE_1st_p90_C3	−0.12	−0.12	0.03	−0.32	−0.08	**−0.32**	0.04	2
I_PE_1st_p95_C1	−0.10	−0.10	0.06	−0.13	−0.45	**−0.33**	0.07	2
I_PE_1st_p95_C2	−0.13	−0.10	0.06	−0.21	−0.37	**−0.42**	0.15	3
I_PE_1st_p95_C3	−0.13	−0.12	0.02	−0.33	−0.14	**−0.32**	0.02	2
I_PE_all_p05_C1	−0.03	−0.05	0.00	−0.05	0.11	−0.11	0.08	0
I_PE_all_p05_C2	−0.05	−0.05	−0.02	−0.10	0.10	−0.17	0.04	0
I_PE_all_p05_C3	−0.02	−0.01	−0.01	−0.10	**0.22**	−0.10	0.05	1
I_PE_all_p10_C1	−0.03	−0.04	0.02	−0.06	0.17	−0.13	0.11	0
I_PE_all_p10_C2	−0.05	−0.04	0.00	−0.10	0.12	−0.16	0.05	0
I_PE_all_p10_C3	−0.04	−0.02	0.00	−0.13	**0.23**	−0.13	0.07	1
I_PE_all_p25_C1	−0.05	−0.05	0.04	−0.09	**0.21**	−0.16	0.09	1
I_PE_all_p25_C2	−0.06	−0.06	0.02	−0.11	0.19	−0.18	0.08	0
I_PE_all_p25_C3	−0.06	−0.04	0.03	−0.18	**0.23**	−0.17	0.09	1
I_PE_all_p50_C1	−0.09	−0.10	0.07	−0.16	0.05	**−0.24**	0.06	1
I_PE_all_p50_C2	−0.10	−0.09	0.07	−0.17	0.15	**−0.27**	0.08	1
I_PE_all_p50_C3	−0.08	−0.05	0.05	**−0.22**	0.18	**−0.22**	0.08	2
I_PE_all_p75_C1	−0.12	−0.14	0.10	**−0.20**	**−0.26**	**−0.33**	0.06	3
I_PE_all_p75_C2	−0.13	−0.12	0.08	**−0.23**	−0.04	**−0.36**	0.10	2
I_PE_all_p75_C3	−0.10	−0.08	0.06	**−0.27**	0.07	**−0.26**	0.05	2
I_PE_all_p90_C1	−0.12	−0.13	0.08	−0.17	**−0.43**	**−0.35**	0.06	2
I_PE_all_p90_C2	−0.13	−0.12	0.07	**−0.25**	**−0.25**	**−0.41**	0.13	3
I_PE_all_p90_C3	−0.11	−0.11	0.04	**−0.31**	−0.02	**−0.30**	0.05	2
I_PE_all_p95_C1	−0.11	−0.11	0.06	−0.14	**−0.45**	**−0.35**	0.07	2
I_PE_all_p95_C2	−0.13	−0.11	0.06	**−0.23**	**−0.31**	**−0.41**	0.14	3
I_PE_all_p95_C3	−0.12	−0.12	0.04	**−0.32**	−0.09	**−0.31**	0.03	2
I_PE_si_p05_C1	−0.12	−0.14	0.10	**−0.20**	**−0.42**	**−0.32**	0.05	3
I_PE_si_p05_C2	−0.15	−0.13	0.04	**−0.25**	**−0.44**	**−0.43**	0.09	3
I_PE_si_p05_C3	−0.18	−0.16	−0.06	**−0.30**	0.02	**−0.39**	−0.11	2
I_PE_si_p10_C1	−0.11	−0.13	0.11	**−0.21**	**−0.45**	**−0.32**	0.05	3
I_PE_si_p10_C2	−0.15	−0.13	0.05	**−0.26**	**−0.46**	**−0.43**	0.08	3
I_PE_si_p10_C3	−0.18	−0.16	−0.04	**−0.32**	−0.01	**−0.39**	−0.10	2
I_PE_si_p25_C1	−0.11	−0.12	0.11	**−0.22**	**−0.50**	**−0.32**	0.06	3
I_PE_si_p25_C2	−0.14	−0.11	0.05	**−0.27**	**−0.49**	**−0.43**	0.09	3
I_PE_si_p25_C3	−0.17	−0.16	0.00	**−0.33**	−0.05	**−0.39**	−0.08	2

Table A2. *Cont.*

Feature *	All Trees	*Pinus resinosa*	*Pinus strobus*	*Pinus sylvestris*	*Picea abies*	*Picea glauca*	*Larix laricina*	Count of Correlations ≥0.2 or <−0.2
I_PE_si_p50_C1	−0.11	−0.12	0.10	−0.20	**−0.53**	**−0.31**	0.06	2
I_PE_si_p50_C2	−0.14	−0.11	0.05	**−0.26**	**−0.50**	**−0.42**	0.10	3
I_PE_si_p50_C3	−0.15	−0.16	0.02	**−0.34**	−0.10	**−0.40**	−0.04	2
I_PE_si_p75_C1	−0.11	−0.10	0.07	−0.15	**−0.50**	**−0.31**	0.06	2
I_PE_si_p75_C2	−0.13	−0.10	0.04	**−0.26**	**−0.48**	**−0.43**	0.12	3
I_PE_si_p75_C3	−0.14	−0.15	0.01	**−0.34**	−0.15	**−0.36**	0.00	2
I_PE_si_p90_C1	−0.09	−0.08	0.05	−0.11	**−0.46**	**−0.30**	0.06	2
I_PE_si_p90_C2	−0.12	−0.09	0.04	**−0.21**	**−0.46**	**−0.42**	0.14	3
I_PE_si_p90_C3	−0.14	−0.14	0.01	**−0.34**	**−0.21**	**−0.34**	0.00	3
I_PE_si_p95_C1	−0.09	−0.08	0.04	−0.10	**−0.44**	**−0.29**	0.05	2
I_PE_si_p95_C2	−0.11	−0.08	0.04	−0.20	**−0.43**	**−0.40**	0.14	2
I_PE_si_p95_C3	−0.14	−0.13	0.01	**−0.34**	**−0.23**	**−0.34**	0.00	3
I_RCG2_1st_mn	−0.03	0.02	−0.08	−0.04	**0.22**	−0.03	−0.02	1
I_RCG2_1st_p50	−0.02	0.03	−0.07	−0.02	0.17	−0.03	−0.01	0
I_RCG2_1st_p75	−0.03	0.02	−0.08	−0.04	**0.23**	−0.03	0.01	1
I_RCG2_1st_p90	−0.04	0.01	−0.08	−0.05	**0.24**	−0.03	0.01	1
I_RCG2_1st_p95	−0.04	0.01	−0.07	−0.05	**0.22**	−0.03	−0.02	1
I_RCG2_all_mn	0.00	0.05	−0.07	−0.02	**0.21**	0.01	0.01	1
I_RCG2_all_p50	0.01	0.04	−0.04	0.01	0.10	0.00	0.03	0
I_RCG2_all_p75	−0.01	0.05	−0.07	−0.01	**0.21**	0.01	0.02	1
I_RCG2_all_p90	−0.02	0.04	−0.08	−0.04	**0.25**	−0.01	0.04	1
I_RCG2_all_p95	−0.03	0.03	−0.07	−0.05	**0.23**	−0.01	0.00	1
I_RCG2_si_mn	−0.09	−0.04	−0.12	−0.12	**0.23**	−0.16	−0.09	1
I_RCG2_si_p50	−0.09	−0.04	−0.11	−0.11	**0.23**	−0.17	−0.08	1
I_RCG2_si_p75	−0.07	−0.02	−0.10	−0.09	**0.22**	−0.10	−0.01	1
I_RCG2_si_p90	−0.06	−0.01	−0.08	−0.09	0.19	−0.07	−0.03	0
I_RCG2_si_p95	−0.06	−0.01	−0.07	−0.08	0.17	−0.06	−0.03	0
I_RM_1st_mn_all_mn_C1	0.01	0.01	0.06	−0.04	**−0.25**	0.00	0.05	1
I_RM_1st_mn_all_mn_C2	0.03	0.05	0.02	−0.05	**−0.27**	0.04	0.11	1
I_RM_1st_mn_all_mn_C3	−0.11	−0.11	0.01	−0.17	**−0.27**	−0.14	−0.03	1
Count of correlations ≥0.2 or < −0.2	0	0	0	56	88	83	0	227

* Individual channel intensity features which did not have at least one correlation value larger than |±0.2| with the mean scan angle in any of the three channels and for any species were not presented in this table, but are listed here: DI_1st_kurt, DI_all_kurt, DI_si_cv, DI_si_kurt, DI_si_skew, IR_all_lm, IR_si_lm, MI_1st_10_90_n_mn, 1st_5_95_n_mn, MI_si_10_90_n_mn, MI_si_5_95_n_mn. The normalized indices NDG1 and NDIR, and ratios RCG1 and RCIR had no correlation value larger than |±0.2| to the mean scan angle for any combinations of return type (all, si, 1st) and statistic (mn, p50, p75, p90, p95). The description of feature names is given in Table 2. The description of feature names is given in Table 2. Correlations values higher than |±0.2| are highlighted in boldface type.

Table A3. Correlations between normalized intensity features and mean scan angle.

Feature *	All Trees	*Pinus resinosa*	*Pinus strobus*	*Pinus sylvestris*	*Picea abies*	*Picea glauca*	*Larix laricina*	Count of Correlations ≥0.2 or <−0.2
I_DI_1st_cv_C1	−0.05	−0.04	−0.05	−0.02	**−0.33**	−0.04	−0.01	1
I_DI_1st_cv_C2	−0.01	−0.02	−0.03	0.04	**−0.21**	0.02	0.03	1
I_DI_1st_cv_C3	−0.08	−0.06	−0.04	−0.09	**−0.37**	−0.08	−0.02	1
I_DI_1st_sd_C1	−0.03	−0.01	0.02	0.02	**−0.22**	0.05	−0.03	1
I_DI_1st_sd_C2	−0.01	0.01	0.06	0.03	−0.08	0.04	0.06	0
I_DI_1st_sd_C3	−0.06	−0.01	−0.03	−0.09	−0.05	−0.04	−0.07	0
I_DI_1st_skew_C1	−0.05	−0.05	−0.10	−0.02	**−0.26**	−0.07	−0.02	1
I_DI_1st_skew_C2	−0.02	−0.01	−0.08	0.02	**−0.21**	−0.02	0.01	1
I_DI_1st_skew_C3	−0.07	−0.06	−0.09	−0.05	**−0.24**	−0.04	−0.05	1
I_DI_all_cv_C1	−0.06	−0.05	−0.02	−0.05	**−0.39**	−0.05	−0.02	1
I_DI_all_cv_C2	0.00	0.01	0.00	0.00	**−0.33**	0.04	0.07	1
I_DI_all_cv_C3	−0.09	−0.07	−0.02	−0.12	**−0.38**	−0.09	−0.01	1
I_DI_all_skew_C1	−0.03	−0.03	−0.07	−0.02	**−0.31**	−0.04	0.01	1
I_DI_all_skew_C2	−0.01	0.00	−0.07	0.00	**−0.33**	0.04	0.05	1
I_DI_all_skew_C3	−0.09	−0.07	−0.10	−0.10	**−0.30**	−0.07	−0.07	1

Table A3. *Cont.*

Feature *	All Trees	*Pinus resinosa*	*Pinus strobus*	*Pinus sylvestris*	*Picea abies*	*Picea glauca*	*Larix laricina*	Count of Correlations ≥0.2 or <−0.2
I_MI_1st_10_90_mn_C1	0.02	0.06	0.09	0.06	0.17	0.12	−0.01	0
I_MI_1st_10_90_mn_C2	0.01	0.03	0.11	−0.02	0.19	0.01	0.05	0
I_MI_1st_10_90_mn_C3	0.01	0.10	0.02	−0.02	**0.34**	0.05	−0.06	1
I_MI_1st_10_90_n_mn_C1	0.03	0.03	0.07	0.01	**0.25**	0.06	0.02	1
I_MI_1st_10_90_n_mn_C2	0.01	0.00	0.06	−0.02	0.17	−0.03	0.00	0
I_MI_1st_10_90_n_mn_C3	0.06	0.06	0.07	0.05	**0.23**	0.03	0.04	1
I_MI_1st_5_95_mn_C1	0.02	0.06	0.09	0.06	0.16	0.13	−0.01	0
I_MI_1st_5_95_mn_C2	0.01	0.03	0.11	−0.02	0.19	0.01	0.05	0
I_MI_1st_5_95_mn_C3	0.01	0.10	0.01	−0.02	**0.34**	0.05	−0.05	1
I_MI_1st_5_95_n_mn_C1	0.04	0.04	0.07	0.01	**0.25**	0.07	0.06	1
I_MI_1st_5_95_n_mn_C2	0.01	0.01	0.06	−0.03	0.16	−0.01	0.00	0
I_MI_1st_5_95_n_mn_C3	0.07	0.06	0.08	0.06	**0.25**	0.06	0.08	1
I_MI_1st_mn_C1	0.02	0.06	0.08	0.06	0.13	0.12	−0.01	0
I_MI_1st_mn_C2	0.01	0.03	0.11	−0.02	0.18	0.01	0.05	0
I_MI_1st_mn_C3	0.00	0.09	0.01	−0.03	**0.33**	0.04	−0.07	1
I_MI_all_10_90_mn_C1	0.02	0.05	0.07	0.08	**0.31**	0.10	−0.03	1
I_MI_all_10_90_mn_C2	0.00	0.01	0.10	0.01	**0.30**	−0.01	0.01	1
I_MI_all_10_90_mn_C3	0.03	0.12	0.02	0.03	**0.39**	0.08	−0.05	1
I_MI_all_10_90_n_mn_C1	0.03	0.03	0.06	0.02	**0.35**	0.04	0.01	1
I_MI_all_10_90_n_mn_C2	0.00	0.00	0.05	0.00	**0.33**	−0.02	−0.05	1
I_MI_all_10_90_n_mn_C3	0.08	0.06	0.07	0.09	**0.30**	0.06	0.06	1
I_MI_all_5_95_mn_C1	0.02	0.05	0.07	0.08	**0.29**	0.11	−0.03	1
I_MI_all_5_95_mn_C2	0.00	0.01	0.10	0.01	**0.29**	−0.01	0.01	1
I_MI_all_5_95_mn_C3	0.03	0.12	0.01	0.03	**0.39**	0.08	−0.05	1
I_MI_all_5_95_n_mn_C1	0.04	0.04	0.07	0.03	**0.33**	0.04	0.02	1
I_MI_all_5_95_n_mn_C2	0.01	0.01	0.05	0.00	**0.31**	−0.03	−0.06	1
I_MI_all_5_95_n_mn_C3	0.08	0.06	0.08	0.11	**0.31**	0.07	0.09	1
I_MI_all_mn_C1	0.01	0.05	0.06	0.08	**0.25**	0.11	−0.03	1
I_MI_all_mn_C2	0.00	0.01	0.10	0.01	**0.28**	−0.01	0.02	1
I_MI_all_mn_C3	0.02	0.12	0.01	0.02	**0.38**	0.08	−0.06	1
I_NDG2_1st_mn	0.03	−0.02	0.08	0.05	**−0.22**	0.04	0.01	1
I_NDG2_1st_p50	0.02	−0.02	0.06	0.02	−0.16	0.04	0.01	0
I_NDG2_1st_p75	0.03	−0.02	0.08	0.05	**−0.22**	0.05	−0.01	1
I_NDG2_1st_p90	0.04	−0.01	0.07	0.06	**−0.23**	0.03	−0.01	1
I_NDG2_1st_p95	0.04	−0.01	0.07	0.06	**−0.21**	0.03	0.02	1
I_NDG2_all_mn	0.00	−0.05	0.06	0.03	**−0.20**	0.00	−0.01	1
I_NDG2_all_p50	−0.01	−0.04	0.04	0.00	−0.10	0.01	−0.03	0
I_NDG2_all_p75	0.01	−0.04	0.07	0.02	**−0.21**	0.00	−0.03	1
I_NDG2_all_p90	0.02	−0.03	0.07	0.05	**−0.24**	0.02	−0.04	1
I_NDG2_all_p95	0.03	−0.03	0.06	0.06	**−0.23**	0.02	0.00	1
I_NDG2_si_mn	0.09	0.04	0.11	0.12	**−0.22**	0.16	0.09	1
I_NDG2_si_p50	0.09	0.04	0.10	0.11	**−0.21**	0.17	0.07	1
I_NDG2_si_p75	0.07	0.02	0.09	0.09	**−0.21**	0.11	0.01	1
I_NDG2_si_p90	0.06	0.01	0.07	0.09	−0.18	0.08	0.02	0
I_NDG2_si_p95	0.06	0.01	0.07	0.08	−0.16	0.07	0.02	0
I_PE_1st_p05_C1	0.02	0.02	0.00	0.02	**0.22**	−0.02	0.02	1
I_PE_1st_p05_C2	−0.01	0.00	0.00	−0.04	0.15	−0.06	0.00	0
I_PE_1st_p05_C3	0.03	0.06	−0.01	0.02	**0.35**	0.02	−0.03	1
I_PE_1st_p10_C1	0.03	0.03	0.02	0.03	**0.27**	0.00	0.02	1
I_PE_1st_p10_C2	0.00	0.01	0.02	−0.04	0.19	−0.04	0.02	0
I_PE_1st_p10_C3	0.04	0.07	−0.01	0.02	**0.38**	0.04	−0.02	1
I_PE_1st_p25_C1	0.03	0.05	0.06	0.04	**0.29**	0.04	0.00	1
I_PE_1st_p25_C2	0.01	0.02	0.06	−0.03	**0.20**	−0.01	0.04	1
I_PE_1st_p25_C3	0.03	0.08	0.01	0.00	**0.36**	0.03	−0.05	1
I_PE_1st_p50_C1	0.02	0.05	0.10	0.05	0.17	0.12	0.00	0
I_PE_1st_p50_C2	0.01	0.03	0.12	−0.02	**0.20**	0.02	0.03	1
I_PE_1st_p50_C3	0.01	0.09	0.03	−0.01	**0.32**	0.05	−0.05	1
I_PE_1st_p75_C1	0.01	0.06	0.09	0.05	0.00	0.15	−0.02	0
I_PE_1st_p75_C2	0.01	0.04	0.12	−0.01	0.12	0.04	0.04	0
I_PE_1st_p75_C3	−0.01	0.08	0.02	−0.04	**0.27**	0.05	−0.05	1
I_PE_1st_p90_C1	0.00	0.03	0.06	0.06	−0.10	0.12	−0.02	0
I_PE_1st_p90_C2	0.01	0.05	0.10	0.02	0.06	0.05	0.06	0
I_PE_1st_p90_C3	−0.02	0.06	0.00	−0.05	**0.21**	0.04	−0.05	1

Table A3. *Cont.*

Feature *	All Trees	*Pinus resinosa*	*Pinus strobus*	*Pinus sylvestris*	*Picea abies*	*Picea glauca*	*Larix laricina*	Count of Correlations ≥0.2 or <−0.2
I_PE_1st_p95_C1	0.00	0.02	0.04	0.05	−0.11	0.11	−0.02	0
I_PE_1st_p95_C2	0.01	0.04	0.10	0.04	0.04	0.07	0.07	0
I_PE_1st_p95_C3	−0.03	0.05	−0.01	−0.06	0.16	0.04	−0.08	0
I_PE_all_p05_C1	0.03	0.03	−0.01	0.08	**0.27**	0.04	0.01	1
I_PE_all_p05_C2	−0.01	−0.01	−0.02	−0.02	0.18	−0.07	−0.02	0
I_PE_all_p05_C3	0.06	0.08	−0.03	0.07	**0.35**	0.07	−0.05	1
I_PE_all_p10_C1	0.04	0.04	0.01	0.09	**0.35**	0.03	0.02	1
I_PE_all_p10_C2	0.00	0.00	0.01	0.00	**0.22**	−0.05	−0.02	1
I_PE_all_p10_C3	0.06	0.09	−0.02	0.07	**0.38**	0.07	−0.04	1
I_PE_all_p25_C1	0.04	0.05	0.02	0.08	**0.40**	0.04	0.00	1
I_PE_all_p25_C2	0.00	0.00	0.03	0.01	**0.30**	−0.03	0.00	1
I_PE_all_p25_C3	0.06	0.10	0.00	0.07	**0.40**	0.08	−0.03	1
I_PE_all_p50_C1	0.02	0.05	0.06	0.06	**0.33**	0.09	−0.03	1
I_PE_all_p50_C2	0.00	0.00	0.09	0.00	**0.31**	−0.02	0.00	1
I_PE_all_p50_C3	0.04	0.12	0.02	0.04	**0.39**	0.08	−0.03	1
I_PE_all_p75_C1	0.01	0.05	0.09	0.06	0.12	0.13	−0.03	0
I_PE_all_p75_C2	0.00	0.02	0.11	0.00	**0.24**	0.03	0.02	1
I_PE_all_p75_C3	0.01	0.11	0.03	0.00	**0.32**	0.08	−0.05	1
I_PE_all_p90_C1	0.00	0.03	0.06	0.06	−0.04	0.13	−0.04	0
I_PE_all_p90_C2	0.01	0.04	0.11	0.02	0.12	0.03	0.04	0
I_PE_all_p90_C3	−0.01	0.08	0.00	−0.03	**0.27**	0.07	−0.05	1
I_PE_all_p95_C1	−0.01	0.01	0.04	0.05	−0.09	0.11	−0.03	0
I_PE_all_p95_C2	0.01	0.04	0.10	0.03	0.08	0.06	0.05	0
I_PE_all_p95_C3	−0.02	0.06	0.00	−0.05	**0.21**	0.05	−0.07	1
I_PE_si_p05_C1	0.00	0.00	0.10	0.02	−0.16	0.02	−0.04	0
I_PE_si_p05_C2	−0.04	−0.03	0.06	−0.07	**−0.21**	−0.12	0.00	1
I_PE_si_p05_C3	−0.11	−0.07	−0.08	−0.15	0.15	**−0.22**	−0.17	1
I_PE_si_p10_C1	0.01	0.02	0.11	0.03	−0.16	0.05	−0.04	0
I_PE_si_p10_C2	−0.03	−0.01	0.08	−0.05	**−0.20**	−0.09	−0.01	1
I_PE_si_p10_C3	−0.11	−0.06	−0.07	−0.15	0.15	−0.20	−0.17	0
I_RCG1_si_mn	−0.10	−0.06	−0.13	−0.07	**0.20**	−0.09	−0.14	1
I_RCG2_1st_mn	−0.03	0.02	−0.08	−0.04	**0.22**	−0.03	−0.01	1
I_RCG2_1st_p50	−0.02	0.02	−0.06	−0.02	0.17	−0.03	−0.01	0
I_RCG2_1st_p75	−0.03	0.02	−0.08	−0.05	**0.23**	−0.04	0.01	1
I_RCG2_1st_p90	−0.04	0.01	−0.08	−0.06	**0.24**	−0.03	0.01	1
I_RCG2_1st_p95	−0.04	0.01	−0.07	−0.05	**0.22**	−0.03	−0.02	1
I_RCG2_all_mn	0.00	0.05	−0.06	−0.02	**0.21**	0.01	0.01	1
I_RCG2_all_p50	0.01	0.04	−0.04	0.00	0.11	0.00	0.03	0
I_RCG2_all_p75	−0.01	0.04	−0.07	−0.01	**0.22**	0.01	0.03	1
I_RCG2_all_p90	−0.02	0.03	−0.08	−0.05	**0.25**	−0.01	0.04	1
I_RCG2_all_p95	−0.03	0.03	−0.06	−0.05	**0.24**	−0.01	0.00	1
I_RCG2_si_mn	−0.09	−0.04	−0.12	−0.12	**0.23**	−0.16	−0.08	1
I_RCG2_si_p50	−0.09	−0.04	−0.10	−0.11	**0.23**	−0.17	−0.07	1
I_RCG2_si_p75	−0.07	−0.02	−0.09	−0.09	**0.22**	−0.10	−0.01	1
I_RCG2_si_p90	−0.06	−0.02	−0.07	−0.09	0.20	−0.07	−0.02	0
I_RCG2_si_p95	−0.06	−0.01	−0.07	−0.08	0.18	−0.06	−0.02	0
I_RM_1st_mn_all_mn_C1	0.01	0.01	0.06	−0.04	**−0.24**	0.00	0.05	1
I_RM_1st_mn_all_mn_C2	0.03	0.05	0.02	−0.05	**−0.27**	0.04	0.11	1
I_RM_1st_mn_all_mn_C3	−0.11	−0.10	0.01	−0.17	**−0.27**	−0.14	−0.03	1
Count of correlations ≥0.2 or <−0.2	0	0	0	0	89	1	0	90

* Individual channel intensity features which did not have at least one correlation value larger than |±0.2| with the mean scan angle in any of the three channels and for any species were not presented in the table, but are listed here: DI_1st_kurt, DI_all_kurt, DI_all_sd, DI_si_cv, DI_si_kurt, DI_si_sd, DI_si_skew, IR_all_lm, IR_si_lm, IR_all_sd, IR_si_lm, IR_si_sd, MI_si_10_90_mn, MI_si_10_90_n_mn, MI_si_5_95_mn, MI_si_5_95_n_mn, MI_si_mn, PE_si_p25, PE_si_p50, PE_si_p75, PE_si_p90, PE_si_p95. The normalized indices NDG1 and NDIR, and the ratio RCIR had no correlation value larger than |±0.2| to the mean scan angle for any combinations of return type (all, si, 1st) and statistic (mn, p50, p75, p90, p95). The same applies for RCG1, except for the combination si_mn. The description of feature names is given in Table 2. The description of feature names is given in Table 2. Correlations values higher than |±0.2| are highlighted in boldface type.

Table A4. Comparison of the classification accuracy capability of different feature categories as a function of scan angle class.

Feature Category	Normalization	Channel	No of Features	Overall Accuracy	Accuracy in Angle Class 1	Accuracy in Angle Class 2	Accuracy in Angle Class 3
3D	N.O.	C1	64	0.60	0.61	0.60	0.58
3D	N.O.	C2	64	0.61	0.61	0.63	0.58
3D	N.O.	C3	64	0.59	0.60	0.57	0.64
3D	N.O.	C321	64	0.64	0.63	0.65	0.61
Intensity	Raw	C1	53	0.54	0.51	0.58	0.53
Intensity	Raw	C2	53	0.43	0.44	0.44	0.40
Intensity	Raw	C3	53	0.58	0.56	0.60	0.59
Intensity	Raw	C1_C2	30	0.40	0.41	0.40	0.40
Intensity	Raw	C1_C3	30	0.37	0.39	0.36	0.36
Intensity	Raw	C2_C3	30	0.50	0.49	0.53	0.47
Intensity	Normalized	C1	53	0.64	0.64	0.68	0.58
Intensity	Normalized	C2	53	0.52	0.52	0.54	0.48
Intensity	Normalized	C3	53	0.64	0.64	0.64	0.61
Intensity	Normalized	C1_C2	30	0.40	0.42	0.40	0.40
Intensity	Normalized	C1_C3	30	0.37	0.38	0.35	0.36
Intensity	Normalized	C2_C3	30	0.51	0.50	0.53	0.47
Intensity	Raw	all	249	0.75	0.75	0.77	0.72
Intensity	Normalized	all	249	0.79	0.78	0.81	0.76
3D + Intensity	Raw	all	505	0.83	0.82	0.84	0.82
3D + Intensity	Normalized	all	505	0.85	0.84	0.86	0.83

References

1. Vauhkonen, J.; Korpela, I.; Maltamo, M.; Tokola, T. Imputation of single-tree attributes using airborne laser scanning-based height, intensity, and alpha shape metrics. *Remote Sens. Environ.* **2010**, *114*, 1263–1276. [CrossRef]
2. Suratno, A.; Seielstad, C.; Queen, L. Tree species identification in mixed coniferous forest using airborne laser scanning. *ISPRS J. Photogramm. Remote Sens.* **2009**, *64*, 683–693. [CrossRef]
3. Lin, Y.; Hyyppä, J. A comprehensive but efficient framework of proposing and validating feature parameters from airborne LiDAR data for tree species classification. *Int. J. Appl. Earth Obs. Geoinf.* **2016**, *46*, 45–55. [CrossRef]
4. Ko, C.; Sohn, G.; Remmel, T.K. Tree genera classification with geometric features from high-density airborne LiDAR. *Can. J. Remote Sens.* **2013**, *39*, S73–S85. [CrossRef]
5. Harikumar, A.; Bovolo, F.; Bruzzone, L. An internal crown geometric model for conifer species classification with high-density LiDAR Data. *IEEE Trans. Geosci. Remote Sens.* **2017**, *55*, 2924–2940. [CrossRef]
6. Vauhkonen, J.; Tokola, T.; Packalén, P.; Maltamo, M. Identification of scandinavian commercial species of individual trees from airborne laser scanning data using alpha shape metrics. *For. Sci.* **2009**, *55*, 37–47. [CrossRef]
7. Ørka, H.O.; Næsset, E.; Bollandsås, O.M. Classifying species of individual trees by intensity and structure features derived from airborne laser scanner data. *Remote Sens. Environ.* **2009**, *113*, 1163–1174. [CrossRef]
8. Prieur, J.-F.; St-Onge, B.; Fournier, R.A.; Woods, M.E.; Rana, P.; Kneeshaw, D. A Comparison of Three Airborne Laser Scanner Types for Species Identification of Individual Trees. *Sensors* **2022**, *22*, 35. [CrossRef]
9. Ørka, H.O.; Gobakken, T.; Næsset, E.; Ene, L.; Lien, V. Simultaneously acquired airborne laser scanning and multispectral imagery for individual tree species identification. *Can. J. Remote Sens.* **2012**, *38*, 125–138. [CrossRef]
10. Liu, L.; Coops, N.C.; Aven, N.W.; Pang, Y. Mapping urban tree species using integrated airborne hyperspectral and LiDAR remote sensing data. *Remote Sens. Environ.* **2017**, *200*, 170–182. [CrossRef]
11. Shi, Y.; Skidmore, A.K.; Wang, T.; Holzwarth, S.; Heiden, U.; Pinnel, N.; Zhu, X.; Heurich, M. Tree species classification using plant functional traits from LiDAR and hyperspectral data. *Int. J. Appl. Earth Obs. Geoinf.* **2018**, *73*, 207–219. [CrossRef]
12. Ørka, H.O.; Dalponte, M.; Gobakken, T.; Næsset, E.; Ene, L.T. Characterizing forest species composition using multiple remote sensing data sources and inventory approaches. *Scand. J. For. Res.* **2013**, *28*, 677–688. [CrossRef]
13. Deng, S.; Katoh, M.; Yu, X.; Hyyppä, J.; Gao, T. Comparison of tree species classifications at the individual tree level by combining ALS data and RGB images using different algorithms. *Remote Sens.* **2016**, *8*, 1034. [CrossRef]
14. Budei, B.C.; St-Onge, B.; Hopkinson, C.; Audet, F.-A. Identifying the genus or species of individual trees using a three-wavelength airborne lidar system. *Remote Sens. Environ.* **2018**, *204*, 632–647. [CrossRef]
15. Yu, X.; Hyyppä, J.; Litkey, P.; Kaartinen, H.; Vastaranta, M.; Holopainen, M. Single-Sensor Solution to Tree Species Classification Using Multispectral Airborne Laser Scanning. *Remote Sens.* **2017**, *9*, 108. [CrossRef]
16. Axelsson, A.; Lindberg, E.; Olsson, H. Exploring Multispectral ALS Data for Tree Species Classification. *Remote Sens.* **2018**, *10*, 183. [CrossRef]

17. St-Onge, B.; Budei, B.C. Individual tree species identification using the multispectral return intensities of the Optech Titan LiDAR system. In Proceedings of the SilviLaser, La Grande Motte, France, 28–30 September 2015; pp. 71–73.
18. Budei, B.C.; St-Onge, B. Variability of multispectral lidar 3D and intensity features with individual tree height and its influence on needleleaf tree species identification. *Can. J. Remote Sens.* **2018**, *44*, 263–286. [CrossRef]
19. Ahokas, E.; Hyyppä, J.; Yu, X.; Liang, X.; Matikainen, L.; Karila, K.; Litkey, P.; Kukko, A.; Jaakkola, A.; Kaartinen, H.; et al. Towards Automatic Single-Sensor Mapping by Multispectral Airborne Laser Scanning. In Proceedings of the 23rd International Archives of the Photogrammetry, Remote Sensing and Spatial Information Sciences Congress (ISPRS 2016), Prague, Czech Republic, 12–19 July 2016. [CrossRef]
20. Holmgren, J.; Nilsson, M.; Olsson, H. Estimation of tree height and stem volume on plots using airborne laser scanning. *For. Sci.* **2003**, *49*, 419–428. [CrossRef]
21. Montaghi, A. Effect of scanning angle on vegetation metrics derived from a nationwide Airborne Laser Scanning acquisition. *Can. J. Remote Sens.* **2013**, *39*, S152–S173. [CrossRef]
22. Næsset, E. Determination of mean tree height of forest stands using airborne laser scanner data. *ISPRS J. Photogramm. Remote Sens.* **1997**, *52*, 49–56. [CrossRef]
23. Arumäe, T.; Lang, M. Estimation of canopy cover in dense mixed-species forests using airborne lidar data. *Eur. J. Remote Sens.* **2018**, *51*, 132–141. [CrossRef]
24. Korhonen, L.; Korpela, I.; Heiskanen, J.; Maltamo, M. Airborne discrete-return LIDAR data in the estimation of vertical canopy cover, angular canopy closure and leaf area index. *Remote Sens. Environ.* **2011**, *115*, 1065–1080. [CrossRef]
25. Korhonen, L.; Morsdorf, F. Estimation of canopy cover, gap fraction and leaf area index with airborne laser scanning. In *Forestry Applications of Airborne Laser Scanning: Concepts and Case Studies*; Maltamo, M., Næsset, E., Vauhkonen, J., Eds.; Springer: Dordrecht, The Netherlands, 2014; pp. 397–417.
26. Liu, J.; Skidmore, A.K.; Jones, S.; Wang, T.; Heurich, M.; Zhu, X.; Shi, Y. Large off-nadir scan angle of airborne LiDAR can severely affect the estimates of forest structure metrics. *ISPRS J. Photogramm. Remote Sens.* **2018**, *136*, 13–25. [CrossRef]
27. Zheng, G.; Ma, L.; Eitel, J.U.H.; He, W.; Magney, T.S.; Moskal, L.M.; Li, M. Retrieving Directional Gap Fraction, Extinction Coefficient, and Effective Leaf Area Index by Incorporating Scan Angle Information From Discrete Aerial Lidar Data. *IEEE Trans. Geosci. Remote Sens.* **2017**, *55*, 577–590. [CrossRef]
28. Bater, C.W.; Wulder, M.A.; Coops, N.C.; Nelson, R.F.; Hilker, T.; Næsset, E. Stability of sample-based scanning-LiDAR-derived vegetation metrics for forest monitoring. *IEEE Trans. Geosci. Remote Sens.* **2011**, *49*, 2385–2392. [CrossRef]
29. Van Lier, O.R.; Luther, J.E.; White, J.C.; Fournier, R.A.; Côté, J.-F. Effect of scan angle on ALS metrics and area-based predictions of forest attributes for balsam fir dominated stands. *For. Int. J. For. Res.* **2022**, *95*, 49–72. [CrossRef]
30. Goodwin, N.R.; Coops, N.C.; Culvenor, D.S. Development of a simulation model to predict LiDAR interception in forested environments. *Remote Sens. Environ.* **2007**, *111*, 481–492. [CrossRef]
31. Morsdorf, F.; Nichol, C.; Malthus, T.; Woodhouse, I.H. Assessing forest structural and physiological information content of multi-spectral LiDAR waveforms by radiative transfer modelling. *Remote Sens. Environ.* **2009**, *113*, 2152–2163. [CrossRef]
32. Disney, M.I.; Kalogirou, V.; Lewis, P.; Prieto-Blanco, A.; Hancock, S.; Pfeifer, M. Simulating the impact of discrete-return lidar system and survey characteristics over young conifer and broadleaf forests. *Remote Sens. Environ.* **2010**, *114*, 1546–1560. [CrossRef]
33. Hopkinson, C. The influence of flying altitude, beam divergence, and pulse repetition frequency on laser pulse return intensity and canopy frequency distribution. *Can. J. Remote Sens.* **2007**, *33*, 312–324. [CrossRef]
34. Korpela, I.; Ørka, H.O.; Hyyppä, J.; Heikkinen, V.; Tokola, T. Range and AGC normalization in airborne discrete-return LiDAR intensity data for forest canopies. *ISPRS J. Photogramm. Remote Sens.* **2010**, *65*, 369–379. [CrossRef]
35. Coren, F.; Sterzai, P. Radiometric correction in laser scanning. *Int. J. Remote Sens.* **2006**, *27*, 3097–3104. [CrossRef]
36. Gatziolis, D. Dynamic range-based intensity normalization for airborne, discrete return lidar data of forest canopies. *Photogramm. Eng. Remote Sens.* **2011**, *77*, 251–259. [CrossRef]
37. Kaasalainen, S.; Hyyppä, H.; Kukko, A.; Litkey, P.; Ahokas, E.; Hyyppä, J.; Lehner, H.; Jaakkola, A.; Suomalainen, J.; Akujärvi, A.; et al. Radiometric calibration of LIDAR intensity with commercially available reference targets. *IEEE Trans. Geosci. Remote Sens.* **2009**, *47*, 588–598. [CrossRef]
38. Kaasalainen, S.; Pyysalo, U.; Krooks, A.; Vain, A.; Kukko, A.; Hyyppä, J.; Kaasalainen, M. Absolute radiometric calibration of ALS intensity data: Effects on accuracy and target classification. *Sensors* **2011**, *11*, 10586–10602. [CrossRef]
39. Okhrimenko, M.; Hopkinson, C. Investigating the consistency of uncalibrated multispectral lidar vegetation indices at different altitudes. *Remote Sens.* **2019**, *11*, 1531. [CrossRef]
40. Okhrimenko, M.; Coburn, C.; Hopkinson, C. Multi-spectral lidar: Radiometric calibration, canopy spectral reflectance, and vegetation vertical SVI profiles. *Remote Sens.* **2019**, *11*, 1556. [CrossRef]
41. Kukkonen, M.; Maltamo, M.; Korhonen, L.; Packalen, P. Multispectral Airborne LiDAR Data in the Prediction of Boreal Tree Species Composition. *IEEE Trans. Geosci. Remote Sens.* **2019**, *57*, 3462–3471. [CrossRef]
42. You, H.; Wang, T.; Skidmore, A.K.; Xing, Y. Quantifying the effects of normalisation of airborne LiDAR intensity on coniferous forest leaf area index estimations. *Remote Sens.* **2017**, *9*, 163. [CrossRef]
43. Yan, W.Y.; Shaker, A. Correction of Overlapping Multispectral Lidar Intensity Data: Polynomial Approximation of Range and Angle Effects. *Int. Arch. Photogramm. Remote Sens. Spat. Inf. Sci.* **2017**, *XLII-3/W1*, 177–182. [CrossRef]

44. Holmgren, J.; Nilsson, M.; Olsson, H. Simulating the effects of lidar scanning angle for estimation of mean tree height and canopy closure. *Can. J. Remote Sens.* **2003**, *29*, 623–632. [CrossRef]
45. Morsdorf, F.; Frey, O.; Meier, E.; Itten, K.I.; Allgöwer, B. Assessment of the influence of flying altitude and scan angle on biophysical vegetation products derived from airborne laser scanning. *Int. J. Remote Sens.* **2008**, *29*, 1387–1406. [CrossRef]
46. Hopkinson, C.; Chasmer, L.; Gynan, C.; Mahoney, C.; Sitar, M. Multisensor and Multispectral LiDAR Characterization and Classification of a Forest Environment. *Can. J. Remote Sens.* **2016**, *42*, 501–520. [CrossRef]
47. Lovell, J.L.; Jupp, D.L.B.; Newnham, G.J.; Coops, N.C.; Culvenor, D.S. Simulation study for finding optimal lidar acquisition parameters for forest height retrieval. *For. Ecol. Manag.* **2005**, *214*, 398–412. [CrossRef]
48. Magnussen, S.; Boudewyn, P. Derivations of stand heights from airborne laser scanner data with canopy-based quantile estimators. *Can. J. For. Res.* **1998**, *28*, 1016–1031. [CrossRef]
49. Roussel, J.R.; Béland, M.; Caspersen, J.; Achim, A. A mathematical framework to describe the effect of beam incidence angle on metrics derived from airborne LiDAR: The case of forest canopies approaching turbid medium behaviour. *Remote Sens. Environ.* **2018**, *209*, 824–834. [CrossRef]
50. Roussel, J.R.; Caspersen, J.; Béland, M.; Thomas, S.; Achim, A. Removing bias from LiDAR-based estimates of canopy height: Accounting for the effects of pulse density and footprint size. *Remote Sens. Environ.* **2017**, *198*, 1–16. [CrossRef]
51. Rowe, J.S. *Forest Regions of Canada*; Canadian Forestry Service: Ottawa, ON, Canada, 1972.
52. Pang, Y.; Lefsky, M.; Sun, G.; Ranson, J. Impact of footprint diameter and off-nadir pointing on the precision of canopy height estimates from spaceborne lidar. *Remote Sens. Environ.* **2011**, *115*, 2798–2809. [CrossRef]
53. Liaw, A.; Wiener, M. Classification and regression by randomForest. *R News* **2002**, *2*, 18–22.